AGU PUBLICATIONS

Global Biogeochemical Cycles

RESEARCH ARTICLE
10.1002/2016GB005488

Key Points:
- In the South Atlantic, biological production was similar over thousands of kilometers, but variable over hundreds of kilometers
- Particulate organic carbon export flux was correlated with gross primary production, but not net community production
- The relationships between these rates may be related to the role of small phytoplankton cells and dissolved organic carbon in export

Supporting Information:
- Supporting Information S1
- Table S1

Correspondence to:
R. H. R. Stanley,
rachel.stanley@wellesley.edu

Citation:
Howard, E. M., C. A. Durkin, G. M. M. Hennon, F. Ribalet, and R. H. R. Stanley (2017), Biological production, export efficiency, and phytoplankton communities across 8000 km of the South Atlantic, *Global Biogeochem. Cycles*, *31*, 1066–1088, doi:10.1002/2016GB005488.

Received 22 JUL 2016
Accepted 11 JUN 2017
Accepted article online 16 JUN 2017
Published online 11 JUL 2017

Biological production, export efficiency, and phytoplankton communities across 8000 km of the South Atlantic

E. M. Howard[1,2,3], C. A. Durkin[4], G. M. M. Hennon[3,5], F. Ribalet[3], and R. H. R. Stanley[6]

[1]Department of Earth and Planetary Sciences, Massachusetts Institute of Technology, Cambridge, Massachusetts, USA, [2]Department of Marine Chemistry and Geochemistry, Woods Hole Oceanographic Institution, Woods Hole, Massachusetts, USA, [3]School of Oceanography, University of Washington, Seattle, Washington, USA, [4]Moss Landing Marine Laboratories, Moss Landing, California, USA, [5]Lamont-Doherty Earth Observatory, Columbia University, Palisades, New York, USA, [6]Department of Chemistry, Wellesley College, Wellesley, Masachusetts, USA

Abstract In situ oxygen tracers (triple oxygen isotope and oxygen/argon ratios) were used to evaluate meridional trends in surface biological production and export efficiency across ~8000 km of the tropical and subtropical South Atlantic in March–May 2013. We used observations of picophytoplankton, nanophytoplankton, and microphytoplankton to evaluate community structure and diversity and assessed the relationships of these characteristics with production, export efficiency, and particulate organic carbon (POC) fluxes. Rates of productivity were relatively uniform along most of the transect with net community production (NCP) between 0 and 10 mmol O_2 m^{-2} d^{-1}, gross primary production (GPP) between 40 and 100 mmol O_2 m^{-2} d^{-1}, and NCP/GPP, a measure of export efficiency, ranging from 0.1 to 0.2 (0.05–0.1 in carbon units). However, notable exceptions to this basin-scale homogeneity included two locations with highly enhanced NCP and export efficiency compared to surrounding regions. Export of POC and particulate nitrogen, derived from sediment traps, correlated with GPP across the transect, over which the surface community was dominated numerically by picophytoplankton. NCP, however, did not correlate with POC flux; the mean difference between NCP and POC flux was similar to published estimates of dissolved organic carbon export from the surface ocean. The interrelated rates of production presented in this work contribute to the understanding, building on the framework of better-studied ocean basins, of how carbon is biologically transported between the atmosphere and the deep ocean.

Plain Language Summary Photosynthesis in the ocean results in the drawdown of atmospheric carbon dioxide. In this study, we use biological and chemical data from a cruise transiting 8000 km of the South Atlantic Ocean in order to study how biological communities in the surface ocean produced oxygen and took up carbon dioxide from the atmosphere in order to grow and how that carbon was consumed or transferred to greater depths away from the atmosphere. Specifically, we used dissolved gases to measure phytoplankton respiration and photosynthesis and sediment traps to collect falling particles; we also determined phytoplankton community structure at 5 m of water depth. This combination of information about the biological community, production, and export across a large region provides insights into the relationships underlying carbon cycling in the South Atlantic.

1. Introduction

Marine systems play an important role in the global carbon cycle as sinks or sources of atmospheric carbon dioxide [*Takahashi et al.*, 2009]. The biologically mediated processes controlling fixation and export of carbon from the euphotic zone to the deep ocean, called the biological carbon pump [*Volk and Hoffert*, 1985], are a major control on atmospheric CO_2. A primary means of transporting organic matter to the deep ocean is through sinking particulate organic carbon (POC) such as cells, detrital aggregates, and zooplankton fecal pellets [*Benitez-Nelson et al.*, 2001; *Ducklow et al.*, 2001]. Dissolved organic carbon (DOC) fluxes are additionally an important component of carbon export to depth [*Hansell et al.*, 2009; *Hansell*, 2013]. Fluxes of POC and DOC out of the surface mixed layer are modulated by community structure and production of phytoplankton and zooplankton [*Boyd and Newton*, 1995; *Boyd and Trull*, 2007; *Lomas and Bates*, 2004; *Guidi et al.*, 2009, 2016]. Plankton community structure is variable across space (meters to ocean basins) and time (hours to decades) and may be an important factor determining the magnitudes of production rates and carbon export and, thus, the efficiency of the biological carbon pump in sequestering carbon to the deep ocean [*Karl et al.*, 2001, 2012; *Vaillancourt et al.*, 2003;

Richardson and Jackson, 2007; *Henson et al.*, 2012]. Studies have described correlations of community structures with patterns of primary production and carbon export in a variety of nutrient regimes [*Pollard et al.*, 2009; *Moreno-Ostos et al.*, 2011; *Lockwood et al.*, 2012; *Cassar et al.*, 2015]. Transition regions between higher and lower nutrient regions can be zones of high biomass and intensified production [*Juranek et al.*, 2012; *Ostle et al.*, 2015] with unique phytoplankton communities distinct from the regions to either side [*Ribalet et al.*, 2010; *Palevsky et al.*, 2013; *Kavanaugh et al.*, 2014a].

Such relationships between physical ocean structure and nutrients, biological community structure, and the biological carbon pump can be combined with the expanding availability of remotely sensed data [*Johnson et al.*, 2009; *McClain*, 2009; *Xing et al.*, 2011] in order to model primary production and carbon export over regional and global scales [*Behrenfeld and Falkowski*, 1997; *Westberry et al.*, 2008; *Uitz et al.*, 2010]. In some parts of the ocean, satellite-informed model results poorly reproduce in situ observations of production and export in terms of both magnitude and variability [*Friedrichs et al.*, 2009; *Emerson*, 2014; *Lee et al.*, 2015; *Świrgoń and Stramska*, 2015; *Palevsky et al.*, 2016], suggesting that there are still gaps in the mechanistic understanding of what drives production and export. The food web approach of *Siegel et al.* [2014] demonstrates that a better understanding of how community structure relates to production can improve model predictions of carbon export [*Stukel et al.*, 2015]. A growing body of literature suggests that physical variability is an important determinant of community structure [*Barton et al.*, 2010], diversity [*Clayton et al.*, 2013, 2014; *Lévy et al.*, 2014, 2015], production [*Nicholson et al.*, 2008; *Estapa et al.*, 2015], and export [*Ayers and Lozier*, 2012].

We evaluate fluxes associated with the biological carbon pump and phytoplankton community structure over scales of hundreds of kilometers to an ocean basin across an 8000 km transect in the western subtropical and equatorial South Atlantic Ocean by combining measurements of gross primary production and net community production rates (from the triple oxygen isotope and oxygen argon ratio natural abundance tracers) with concurrent in situ high-resolution measurements of surface cyanobacteria and picoeukaryote abundances (underway flow cytometry), surface nanophytoplankton and microphytoplankton abundances (visual microscopy), and POC export fluxes below the surface mixed layer (drifting subsurface sediment traps). GPP is equal to total photosynthetic production prior to any respiration or other recycling of oxygen or organic carbon [*Williams*, 1993]. Net community production (NCP) is equal to GPP minus community respiration and expresses the net carbon drawdown or oxygen production by the biological pump. NCP should be balanced by export of carbon over sufficient scales of time and space [*Emerson et al.*, 1997; *Brix et al.*, 2006], including DOC and zooplankton-mediated export in addition to POC sinking out of the mixed layer [*Emerson*, 2014]. The NCP/GPP ratio is a measure of metabolic efficiency akin to the *f*-, *e*-, and *ef*-ratios [*Eppley and Peterson*, 1979; *Murray et al.*, 1996; *Laws et al.*, 2000] and has been called an "export ratio in O_2 currency" [*Juranek and Quay*, 2013]. Higher NCP/GPP ratios indicate that a larger fraction of production escapes being respired locally over the residence time of the oxygen-based tracers.

In particular, we evaluate (1) how phytoplankton community structure and diversity may relate to production and export, (2) whether differences in net community production and particulate organic carbon export rates are potentially balanced by dissolved organic carbon production, and (3) if export is proportional to autotroph production (GPP) in a transect where picophytoplankton numerically dominate the phytoplankton community [*Richardson and Jackson*, 2007; *Stukel and Landry*, 2010; *Guidi et al.*, 2016].

2. Methods

All samples were collected aboard the R/V *Knorr* (KN210-04). The cruise traversed 8480 km and 22° of latitude of the western South and equatorial Atlantic (Figure 1) between Montevideo, Uruguay, and Bridgetown, Barbados from 25 March through 9 May 2013, in austral fall. This transect encompasses a number of surface physical regimes, including the South Atlantic subtropical front and transition region, subtropical gyre, and the tropics and equatorial current system [*Tsuchiya et al.*, 1994; *Stramma and Schott*, 1999; *Mémery et al.*, 2000]. Finally, the cruise passed through the pelagic and mesohaline portions of the Amazon River plume [*Hu et al.*, 2004]. These physically defined regions overlap distinct biogeographic provinces [*Longhurst*, 1995], including the south subtropical transition zone (SST), the South Atlantic gyre (SAG), the western tropical Atlantic (WTA) and the Amazon River plume (ARP).

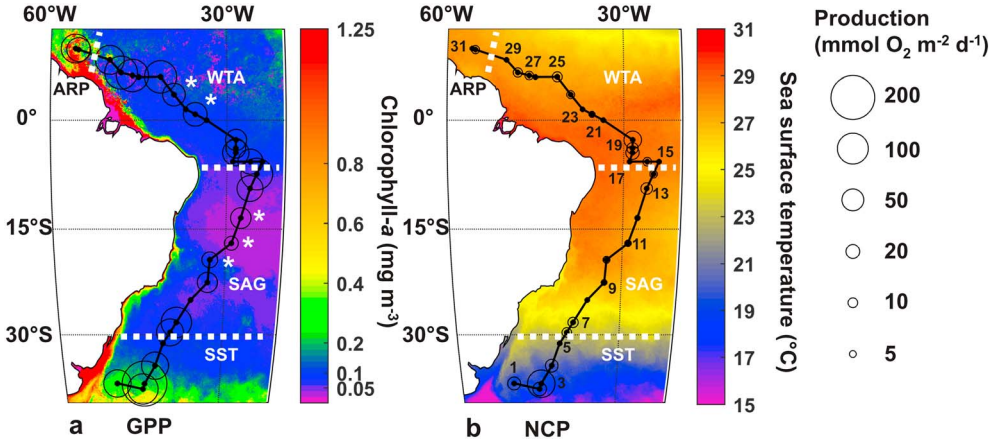

Figure 1. (a) Sample locations and rates of gross primary production (GPP; open circles) in the equatorial and South Atlantic overlaid on satellite-derived March–May mean sea surface chlorophyll *a*, and (b) net community production (NCP) overlaid on daytime sea surface temperature. Locations (black dots) marked with asterisks in Figure 1a are more than 2° latitude from the nearest depth profile (see section 2.2.1), and odd location numbers are labeled in Figure 1b. Production rates were not determined at all sample locations. Four biogeographic provinces are identified as in the text (south subtropical transition zone, SST; South Atlantic gyre, SAG; western tropical Atlantic, WTA; Amazon River plume, ARP) and separated by white dashed lines. Sea surface data are from MODIS-Aqua satellite and obtained from the Giovanni online data system [*Acker and Leptoukh*, 2007; http:Giovanni.gsfc.nasa.gov/Giovanni/] maintained by the NASA Goddard Earth Science Data and Information Services Center.

Samples for gas tracer analysis were collected from surface waters while underway and at discrete stations (Table S1 in the supporting information). At stations with longer sampling durations, samples were collected either at arrival and departure from the station or as time series. Gas tracer estimates of production were compared with concurrent underway observations of surface cyanobacterial and picoeukaryote populations [*Hennon*, 2015]. Data were also compared with concurrent observations of surface eukaryotic phytoplankton abundance and the phytoplankton and carbon fluxes captured in free-floating particle interceptor traps at 125 m reported by *Durkin et al.* [2016]. Particulate nitrogen (PN) fluxes analyzed simultaneously with POC were not previously reported but analyzed as in *Durkin et al.* [2016].

2.1. Underway Sampling Line

Surface water was collected using the ship's underway flow-through system at 5 m depth and passed through an inline de-bubbler and a Seabird Electronics SBE45 thermosalinograph prior to sample collection. In order to minimize biofouling, the underway line was flushed with bleach at the beginning and halfway through the cruise (3 April 2013) by dissolving 150–200 g pelletized sodium hypochlorite in the ~150 L sea chest (~0.1% solution, after *Juranek et al.* [2010]). After each cleaning, the underway line was then flushed with flowing seawater for 12–15 h prior to commencing sampling. Water (1 L min^{-1}) from the underway line was diverted for sampling of gas tracers, nutrients, and chlorophyll *a*.

2.2. Discrete Gas Tracer Theory, Sampling, and Analysis

2.2.1. O_2/Ar and Triple Oxygen Isotope Ratio Theory and Calculation of Production Rates

We use the oxygen to argon ratio as a tracer of net oxygen production in the surface mixed layer. Argon acts as a biologically inert analogue of oxygen in seawater, and the difference in saturation state between the two gases is assumed to correspond primarily to the balance of photosynthesis and respiration [e.g., *Craig and Hayward*, 1987; *Spitzer and Jenkins*, 1989; *Emerson et al.*, 1991]. Extending the equations by *Cassar et al.* [2011] such that argon is not assumed to be at saturation and neglecting horizontal and vertical mixing, the time evolution of oxygen relative to argon in the mixed layer is controlled by production and gas exchange:

$$z\frac{\partial}{\partial t}\left(\mathrm{O_2}\left[\frac{\Delta \mathrm{O_2}}{\mathrm{Ar}}\right]\left[\frac{\mathrm{Ar}}{\mathrm{Ar}_{\mathrm{sat}}}\right]\right)\rho_{\mathrm{sw}} = \mathrm{NCP} - k_{\mathrm{O2}}\mathrm{O_{2\ sat}}\left[\frac{\Delta \mathrm{O_2}}{\mathrm{Ar}}\right]\left[\frac{\mathrm{Ar}}{\mathrm{Ar}_{\mathrm{sat}}}\right]\rho_{\mathrm{sw}} \quad (1)$$

where z is the mixed layer depth defined as a 0.125 kg m^{-3} offset in potential density from the surface [*Levitus*, 1982], O_2 and Ar are measured concentrations (molal), and O_{2sat} and Ar_{sat} are saturation

concentrations (molal) [*Garcia and Gordon*, 1992, 1993; *Hamme and Emerson*, 2004]. The ratio $\Delta O_2/Ar = [(O_2/Ar)/(O_2/Ar)_{saturation} - 1] \times 100\%$ reflects the net biological oxygen production or consumption [*Hendricks et al.*, 2004; *Kaiser et al.*, 2005]. In particular, the "measured" Ar is actually derived from the measured O_2 and O_2/Ar. NCP is an areal rate (mol O_2 m^{-2} d^{-1}), and ρ_{sw} is the in situ density of seawater. k_{O2} is the gas transfer coefficient (m d^{-1}) calculated from 6 h NCEP/NCAR Reanalysis winds [*Kalnay et al.*, 1996] for the cruise track from March to May 2013 using the gas exchange parameterization of *Stanley et al.* [2009] and the 60 day weighting scheme of *Reuer et al.* [2007]. The relationship between wind speed and gas exchange is constrained to ~±15–20% [*Stanley et al.*, 2009; *Ho et al.*, 2011; *Wanninkhof*, 2014] and is in general the largest source of error in resulting NCP rates.

The triple isotope composition of dissolved oxygen is related to photosynthetic oxygen production and is largely independent of respiration. *Juranek and Quay* [2013] discuss the theory, advantages, and limitations of this method in detail. Measured stable oxygen isotope ratios ($^{18}O/^{17}O/^{16}O$) can be used to define the triple oxygen isotope tracer $^{17}\Delta$ in order to conceptualize the relative contribution of photosynthetic oxygen to different water samples, with greater values indicating increased rates of production relative to gas exchange with the atmosphere. In this work we use the definition $^{17}\Delta = (\ln[(^{17}O/^{16}O)_{measured}/(^{17}O/^{16}O)_{air}] - \lambda \ln[(^{18}O/^{16}O)_{measured}/(^{18}O/^{16}O)_{air}]) \times 10^6$ per meg [*Angert et al.*, 2003] relative to an atmospheric oxygen standard, where $\lambda = 0.518$ is the ratio of the mass-dependent isotope enrichment factors for $^{17}O/^{16}O$ and $^{18}O/^{16}O$. Gross primary production (mmol O_2 m^{-2} d^{-1}) is calculated for the surface mixed layer in terms of a balance between gas exchange and production using the oxygen isotope ratios and λ. If the measured $^{17}O/^{16}O$ and $^{18}O/^{16}O$ ratios are notated as ^{17}X and ^{18}X:

$$z\frac{\partial}{\partial t}\left(O_2{}^{17}\Delta\right)\rho_{sw} = GPP\left(\frac{{}^{17}X_P - {}^{17}X}{{}^{17}X} - \lambda\frac{{}^{18}X_P - {}^{18}X}{{}^{18}X}\right) - k_{O2}O_{2\ sat}\left(\frac{{}^{17}X - {}^{17}X_{sat}}{{}^{17}X} - \lambda\frac{{}^{18}X - {}^{18}X_{sat}}{{}^{18}X}\right)\rho_{sw} \quad (2)$$

where ${}^{i}X_P$ is the photosynthetic production ratio and ${}^{i}X_{sat}$ the saturated equilibrium ratio for each isotope (Table S2). Alternate choices for ${}^{i}X_P$ and ${}^{i}X_{sat}$ and λ may be appropriate under some circumstances [*Kaiser*, 2011; *Nicholson*, 2011; *Kaiser and Abe*, 2012]. The above equation is identical to equation (S8) in the supporting information to *Prokopenko et al.* [2011] and neglects fractionation effects during gas exchange and bubble fluxes [*Kaiser*, 2011].

Nicholson et al. [2014] suggest including corrections to equation (2) to account for seasonal entrainment and mixing across the base of the thermocline (e.g., left side of equation (2) becomes $z(\partial/\partial t)(O_2{}^{17}\Delta)\rho_{sw} - C_{GPP}$). These corrections are expressed as the tracer difference from an appropriate point measured below the mixed layer multiplied by the entrainment $\partial z/\partial t$ (only when the mixed layer deepens) and mixing rate $K_z/(z_d - z)$, where K_z is the vertical diffusivity coefficient (m^2 d^{-1}) across the thermocline at z_d, the depth of the sub-mixed layer sample. We apply the same approach to calculating NCP from O_2 and Ar. Simplifying the expressions of *Nicholson et al.* [2014] in terms of measured variables (see supporting information Text S1), we obtain corrections C_{NCP} and C_{GPP} for equations (1) and (2):

$$C_{NCP} = \left(\frac{\partial z}{\partial t} + \frac{K_z}{(z_d - z)}\right)\left(O_{2\ sat}\left[\frac{O_{2\ d} - O_2}{O_{2\ sat}} - \frac{Ar_{\ d} - Ar}{Ar_{\ sat}}\right]\right)\rho_{sw} \quad (3)$$

$$C_{GPP} = \left(\frac{\partial z}{\partial t} + \frac{Kz}{(z_d - z)}\right)O_{2d}\left(\left[\frac{{}^{17}X_d}{{}^{17}X} - 1\right] - \lambda\left[\frac{{}^{18}X_d}{{}^{18}X} - 1\right]\right)\rho_{sw} \quad (4)$$

where the d subscript refers to measurements below the base of the mixed layer (~20 m below the mixed layer depth). Entrainment is estimated from the Monthly Isopycnal and Mixed-layer Ocean Climatology [*Schmidtko et al.*, 2013] based on Argo profiler data, and $\partial z/\partial t$ is set to zero for a shoaling mixed layer. K_z is estimated to have a lower bound of 1.0×10^{-5} m^2 s^{-1} (8.6×10^{-1} m^2 d^{-1}) across the bottom of the mixed layer based on direct measurements along a similar transect at the same time of year [*Mouriño-Carballido et al.*, 2011]. The time rate of change terms generally cannot be evaluated using the

discrete gas samples, so steady state is assumed and equations (1) and (2) are solved for NCP and GPP as follows:

$$\mathrm{NCP} = k_{\mathrm{O2O2\ sat}}\left[\frac{\Delta \mathrm{O_2}}{\mathrm{Ar}}\right]\left[\frac{\mathrm{Ar}}{\mathrm{Ar_{sat}}}\right]\rho_{\mathrm{sw}} - C_{\mathrm{NCP}} \quad (5)$$

$$\mathrm{GPP} = \left[k_{\mathrm{O2O2\ sat}}\left(\frac{^{17}\mathrm{X} - {}^{17}\mathrm{X_{sat}}}{^{17}\mathrm{X}} - \lambda\frac{^{18}\mathrm{X} - {}^{18}\mathrm{X_{sat}}}{^{18}\mathrm{X}}\right)\rho_{\mathrm{sw}} - C_{\mathrm{GPP}}\right] / \left(\frac{^{17}\mathrm{X_P} - {}^{17}\mathrm{X}}{^{17}\mathrm{X}} - \lambda\frac{^{18}\mathrm{X_P} - {}^{18}\mathrm{X}}{^{18}\mathrm{X}}\right) \quad (6)$$

This calculation of GPP and NCP is independent of mixed layer depth except for the effect of entrainment. The potential roles of upwelling and surface divergence on these rates are not accounted for. To calculate NCP and GPP for sample locations without depth profiles, sub-mixed layer values of $\Delta O_2/Ar$ (and thus Ar/Ar_{sat}), $^{17}\Delta$, and ^{17}X were approximated using weighted-mean averaging from adjacent casts. Oxygen profiles at the sample locations were additionally used to constrain likely subsurface values of $\Delta O_2/Ar$. Five locations (noted in Figure 1) are separated from the nearest depth profiles by more than 2° latitude, and interpolating sub-mixed layer $\Delta O_2/Ar$ for entrainment and mixing corrections introduces additional uncertainty in the rate of NCP; the dynamic range of the tracer values immediately below the mixed layer is five times greater for $\Delta O_2/Ar$ relative to its uncertainty than for $^{17}\Delta$.

We address probable systematic biases introduced in the gas mass balances for NCP and GPP in the supporting information Text S2. These include lateral advection [*Peterson and Stramma*, 1991; *Lumpkin and Garzoli*, 2005; *Brandt et al.*, 2006], upwelling [*Helber et al.*, 2007; *Grodsky et al.*, 2008; *Rhein et al.*, 2010; *Kadko and Johns*, 2011], and greater vertical diffusivity [*Carr et al.*, 1992; *Law et al.*, 2003; *Wunsch and Ferrari*, 2004; *Haskell et al.*, 2015]. Most assumptions above are reasonable for this data set. However, diel cycles of the gas tracers [*Sarma et al.*, 2006; *Ferrón et al.*, 2015; *Nicholson et al.*, 2015] can lead to large errors in steady-state production rates as calculated above (as high as ±50%; Figure S1) if samples are taken during daily periods of peak tracer accumulation and deficit [*Hamme et al.*, 2012]. While this is not a major bias in this data set (supporting information Text S1 and Figure S2), it may be an important source of error in other studies when it is not possible to sample multiple timepoints within a given day.

2.2.2. Conversion Between Oxygen and Carbon Units

Oxygen-based rates of NCP and GPP may be converted to carbon units for comparison with other studies. For NCP the ratio of oxygen production to carbon uptake during photosynthesis is expected to be $O_2/C = 1.4$ for nitrate-based production and 1.1 for growth on ammonia [*Laws*, 1991], or 1.0–1.2 for nitrogen fixation-supported growth [*Kirk*, 1994]. A relationship exists between carbon-based net primary production (NPP, GPP minus autotrophic respiration [*Falkowski et al.*, 2003]) estimated from 24 h radiocarbon incubations and ^{18}O incubation based GPP [*Marra*, 2002] or water column triple oxygen isotope based GPP [*Nicholson et al.*, 2012]; the ratio of GPP (moles of oxygen)/NPP (moles carbon) is roughly 2.7 across several ocean regions and experiments [*Juranek and Quay*, 2013, and references therein]. This conversion ratio may vary in space and time [*Nicholson et al.*, 2012] but is generally found to be around the theoretical values of 2.8 [*Juranek and Quay*, 2013] to 3.3 (when biomass normalized; *Halsey et al.* [2010]). With the exception of the ratio reported in *Halsey et al.* [2010], the reported ratios are based on measurements of radiocarbon in filtered particles and implicitly neglect production of DOC and thus may underestimate NPP. We use a ratio of 2.7 to compare our rates to rates of radiocarbon uptake into particles in other studies, but many of those incubations were shorter than 24 h and thus may have lower and less well-defined conversion factors, and the shorter incubations may not approximate NPP but rather a value in between NPP and GPP [*Dring and Jewson*, 1982; *Williams and Lefèvre*, 1996; *Behrenfeld et al.*, 2008; *Marra*, 2009; *Halsey et al.*, 2010]. Combining the conversion of NCP to carbon units and GPP to NPP leads to a form equivalent to the *e*-ratio ([NCP/(1.1 to 1.4)]/[GPP/2.7] = NCP/NPP) in carbon units.

2.2.3. Gas Tracer Sampling

Discrete seawater samples were collected for analysis of O_2 concentration, O_2/Ar ratio, and triple oxygen isotope ratios from Niskin bottles on the conductivity temperature depth (CTD) rosette at cast locations and from the underway line between cast stations. O_2 concentration was generally sampled in replicate following Joint Global Ocean Flux Study protocols [*Knap et al.*, 1996] and titrated after equilibrating to room temperature by a modified amperometric Winkler titration [*Carpenter*, 1965a, 1965b; *Knapp et al.*, 1989]. Full water column profiles of O_2 were collected during stationary cast sampling throughout the cruise in order to calibrate the oxygen sensor on the SBE911+. At a subset of the stations, depth profiles below the mixed layer

were sampled for O_2/Ar and triple oxygen isotope ratios simultaneously with oxygen concentration. The O_2/Ar and triple oxygen isotope ratios in dissolved oxygen were sampled using custom-made evacuated 500 mL glass flasks with gas-tight valves prepoisoned with mercuric chloride [*Emerson et al.*, 1995]. The spatial scale associated with underway samples ranged from stationary sampling to integration over ~3 km depending on ship's speed.

2.2.4. O_2/Ar and Triple Oxygen Isotope Ratio Analytical Methods

Discrete water samples were analyzed for both dissolved O_2/Ar and triple oxygen isotope ratios at Woods Hole Oceanographic Institution using methods similar to those of *Barkan and Luz* [2003]. Sample water and gas headspace were equilibrated at room temperature and the headspace further processed on an automated line which collected O_2 and Ar while separating and discarding water vapor and N_2 [*Stanley and Howard*, 2013]. The O_2 and Ar were passed to a Thermo Scientific MAT 253 isotope ratio mass spectrometer and the O_2/Ar, $^{17}O/^{16}O$, and $^{18}O/^{16}O$ ratios determined. Samples were referenced to a gas secondary standard with similar O_2/Ar to seawater (Scott Specialty Gases). Additionally, equilibrated water and atmospheric air standards (Woods Hole beach air stored in a valved 2 L electropolished stainless steel cylinder) were analyzed every nine samples.

All samples were corrected for the effects of interactions with Ar and trace N_2 at the ion source [*Abe and Yoshida*, 2003] and sample size [*Stanley et al.*, 2010], with corrections applied both on $^{17}O/^{16}O$ and $^{18}O/^{16}O$ directly and on $^{17}\Delta$. Since the Ar corrections were more linear for $^{17}O/^{16}O$ and $^{17}\Delta$, we recalculated $^{18}O/^{16}O$ from those measurements, which was especially important for low O_2 (i.e., high relative Ar) samples. Recalculated values of $^{18}O/^{16}O$ were on average 2×10^{-3} per mil lower than the measured ratio in this data set. Water standards run concurrently with our samples (13 replicates over 19 days) were precise to 0.1% in ΔO_2/Ar, 9×10^{-3} per mil in $^{17}O/^{16}O$, 15×10^{-3} per mil in $^{18}O/^{16}O$, and 3 per meg in $^{17}\Delta$ (3×10^{-3} per mil). Sample duplicate precision was 0.1% in ΔO_2/Ar and 5 per meg in $^{17}\Delta$ (5 pairs from either cast or underway samples).

2.3. Nutrient and Chlorophyll *a* Concentrations

Nutrients were collected from the ship's underway line simultaneously with dissolved gas samples and filtered through 0.2 μm sterile syringe filters (surfactant-free cellulose acetate, Corning). Additional, unfiltered samples were collected from 5 m Niskin bottles during CTD rosette casts [*Kujawinski and Longnecker*, 2014]. Both sample sets were photometrically analyzed on a Technicon Autoanalyzer II at Oregon State University following the methods of *Gordon et al.* [1993]. The nitrite and total nitrate plus nitrite concentrations used in this study from both filtered and unfiltered data sets showed no evidence of systematic bias. Phosphate and ammonia concentrations did have systematic offsets between filtered and unfiltered data sets and thus are not evaluated in this study. Chlorophyll *a* samples were collected from the underway system at each sample location; two pairs of duplicate samples (four samples total) were filtered sequentially at 10 μm and 0.2 μm (polycarbonate, Millipore). Chlorophyll *a* was extracted with 90% acetone and then determined fluorometrically on a Trilogy fluorometer (Turner) according to the methods of *Arar and Collins* [1997]. Blank filters were collected in the same manner using 0.2 μm filtered seawater from the same location to correct for the effects of colored dissolved organic matter on fluorescence measurements.

2.4. Phytoplankton Diversity and Community Structure at 5 m Water Depth

The concentration (cells L^{-1}) of phytoplankton communities of picoplankton (0.5–2 μm) populations identified by continuous underway flow cytometry (reported in *Hennon* [2015]) and of nanoplankton and microplankton (~5 μm and 20–200 μm) identified by light microscopy (reported in *Durkin et al.* [2016]) were used to assess community structure and diversity in the surface waters of the transect (phytoplankton collected at 5 m water depth). In brief, *Prochlorococcus*, *Synechococcus*, and picoeukaryote abundances were identified based on characteristic fluorescence and light scattering [*Ribalet et al.*, 2010; *Swalwell et al.*, 2011]. For this study, continuous data and associated statistics were averaged over the 30 min surrounding discrete underway sampling or, if stationary, over the duration of particle trap deployment, in order to integrate over a similar time and space resolution as the underway gas sampling. Surface phytoplankton abundances reported by *Durkin et al.* [2016] at the same locations as trap deployments were quantified by light microscopy from 0.5 L samples. Microphytoplankton morphotypes were identified to the genus level where possible.

Surface community structure associations were identified using principal component analysis (PCA) on the phytoplankton abundances normalized to variance, and locations with distinct community structures were identified by *k*-means clustering of PCA coordinates using tools in R software (FactoMineR package, R project [*Lê et al.*, 2008]). The number of clusters used in the analysis was determined by identifying the fewest number of clusters that explained a large fraction of total variance. To determine which principal components defined the clustering of similar communities, dominant principal component coordinates of each cluster were identified (cluster coordinate magnitudes accounting for >50% of the absolute magnitude). The phytoplankton with the greatest variable loadings on the dominant principal coordinates of each cluster were identified to determine which phytoplankton influenced the clustering of locations. Additionally, the Shannon-Weaver diversity index (*H*) was calculated from cell concentrations (separated by phytoplankton type, above, e.g., *Prochlorococcus*, genus level microphytoplankton) in R software (vegan package, R project [*Oksanen et al.*, 2016]). Community structure and diversity were only evaluated at locations with microscopy data in addition to continuous flow cytometry observations.

2.5. Biogeographic Provinces

All sample types were grouped by biogeographic province using a clustering approach informed by average daily sea surface temperature, salinity, and chlorophyll *a* fluorescence (in the manner of *Reygondeau et al.* [2013] and *Kavanaugh et al.* [2014b]) as reported in *Hennon* [2015]. Clustered sample locations were then assigned names corresponding to the regions identified by *Longhurst* [1995]. Biogeographic provinces in this data set (Figure 1) include the SST region, the SAG, and the WTA. An additional warm, low salinity, very high chlorophyll *a* fluorescence cluster of samples specific to the mesohaline ARP in this study is grouped separately from the other locations in the WTA. The identified provinces roughly correspond to physical circulation features of the surface ocean, such as the subtropical/subpolar frontal region, subtropical gyre, and equatorial current systems [e.g., *Peterson and Stramma*, 1991].

2.6. Other Statistical Tests

We evaluated correlations between production rates, particle export, phytoplankton abundances, and hydrographic variables throughout the transect and between biogeographic provinces. We calculated Pearson linear correlation coefficients (r) pairwise between each variable. Normality of the data could not be assumed because of limited overlap between data sets and the small number of sample locations across the transect (n = 9 to 30 for each variable). Therefore, we additionally calculated the nonparametric Spearman's rank correlation coefficient (ρ), in which higher ranks correspond to variable pairs that increase monotonically with respect to each other without assuming a linear dependency. Significance was assigned with the standard value of $\alpha = 0.05$ [*Fisher*, 1956].

In order to quantify whether average properties differ significantly between biogeographic provinces, we used the nonparametric equivalent of an ANOVA, the Kruskal-Wallis test [*Kruskal and Wallis*, 1952; *Meyer and Seaman*, 2013] with $\alpha = 0.05$ and the Dunn-Šidák correction [*Šidák*, 1967] for multiple comparisons (more precisely, the median is compared in rank-based tests). We used the non-parametric *k*-sample Anderson-Darling test [*Scholz and Stephens*, 1987; *Trujillo-Ortiz et al.*, 2007] to evaluate whether the sample distribution differed significantly between regions. Finally, we tested whether the variance of each property varied between regions using the Brown-Forsythe test [*Brown and Forsythe*, 1974], a non-parametric equivalent of the *F* test that allows dissimilar sample distributions. Statistical analyses were performed using MATLAB software (release 2015b, *MathWorks* [2015], Natick, MA, USA).

3. Results

Results from this work are summarized below and are tabulated in the supporting information. Depth profile data are presented in Table S2, while surface results from this work and the previously reported results in *Durkin et al.* [2016] and *Hennon* [2015] are presented in Table S3. Oxygen concentrations and CTD data are accessible online (http://www.bco-dmo.org/project/2204; *Kujawinski and Longnecker* [2014]). In Table S3, all results are averaged by sample location, including over multiday periods. The number of replicates, standard deviation of measurements (or counting uncertainty in the case of microscopy samples), and details of uncertainty calculations are reported in Table S3 as well.

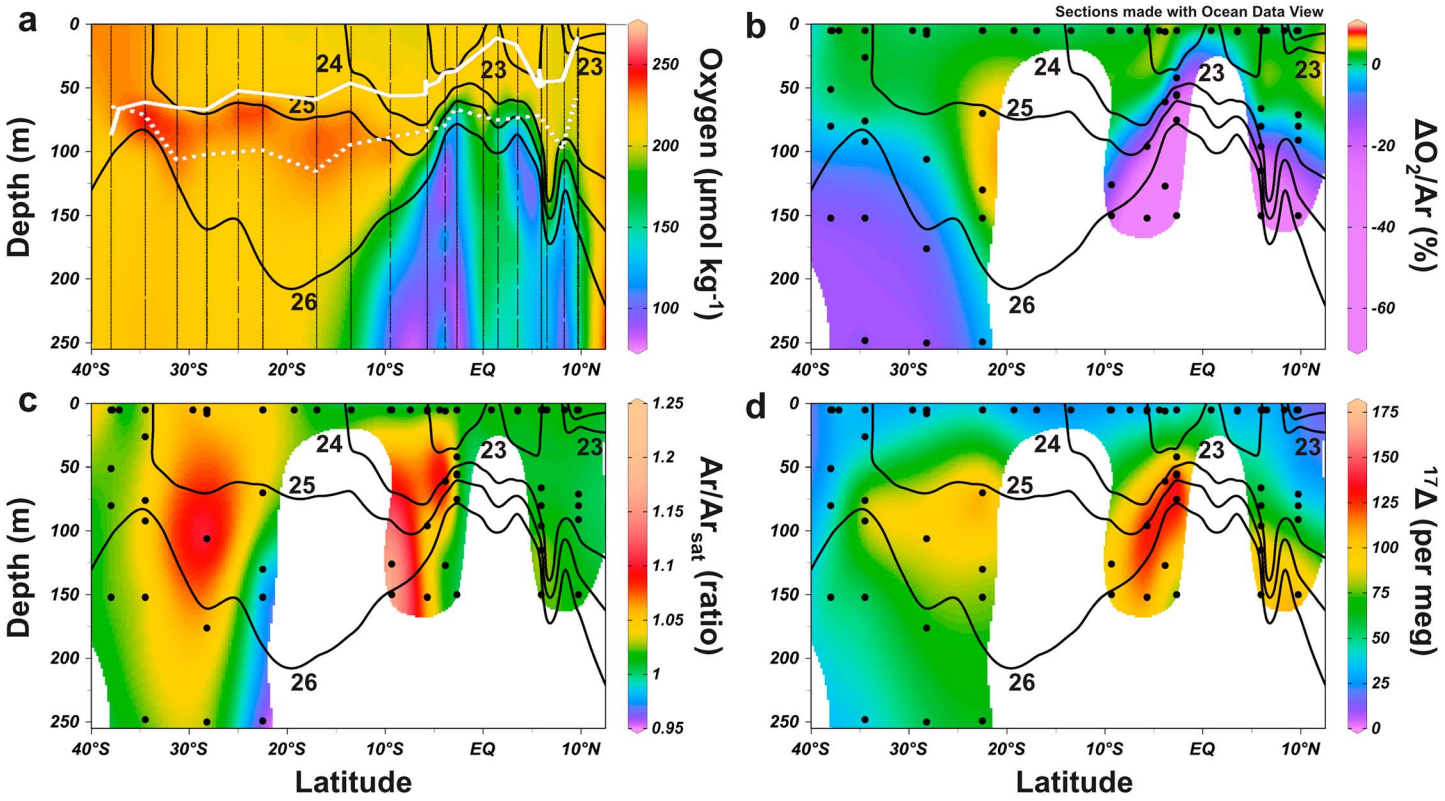

Figure 2. Meridional sections of (a) oxygen concentration, (b) biological oxygen saturation state $\Delta O_2/Ar$ (supersaturation or undersaturation relative to atmospheric equilibrium), (c) argon saturation relative to atmospheric equilibrium Ar/Ar_{sat}, and (d) the triple oxygen isotope tracer $^{17}\Delta$ (relative to the value of atmospheric oxygen). Sample locations are identified as black circles Sample locations are identified as black circles (except in Figure 2a where O_2 profiles from calibrated CTD are denoted by vertical lines), and labeled black contours are isopycnals of neutral density. Mean mixed layer depth (solid white line) and euphotic zone depth (dashed white line) at each location are also plotted in Figure 2a. Sections are gridded with horizontal and vertical length scales of 1° latitude and 20 m depth using Data-Interpolating Variational Analysis in Ocean Data View [*Schlitzer*, 2015; http:odv.awi.de]. Tracer values from the first sample location along the transect (37.1°S, 49.9°W) are not plotted so that latitude increases monotonically along the section.

3.1. Gas Tracers

3.1.1. Surface and Subsurface Gas Tracers

Gas tracer results in the surface 250 m are plotted in Figure 2. Oxygen concentrations were highest in the SST and immediately below the mixed layer of the SAG. This sub-mixed layer maximum was also associated with increased $\Delta O_2/Ar$ and $^{17}\Delta$ that likely accumulated during production within the euphotic zone but below the mixed layer [*Hendricks et al.*, 2005; *Howard et al.*, 2010]—such production is not included in gas tracer based production estimates for the surface mixed layer but is likely around 10–30% of total euphotic zone production (section 5.1). Surface $\Delta O_2/Ar$ and Ar/Ar_{sat} were generally slightly in excess of atmospheric equilibrium because of biological production and bubble dissolution processes [e.g., *Nicholson et al.*, 2011]. The shoaling pycnoclines in the equatorial region were associated with low oxygen concentration, decreased $\Delta O_2/Ar$, increased Ar saturation state (south of the equator), and high $^{17}\Delta$. Ar supersaturations of up to 18% below the mixed layer may result from temperature differences between mixing water masses and the nonlinear response of saturation state to diapycnal mixing [*Gehrie et al.*, 2006; *Ito et al.*, 2007; *Emerson et al.*, 2012].

Underway and cast gas tracer samples were compared to verify that processes within the underway sampling line did not bias gas tracer measurements. No systematic bias in either $\Delta O_2/Ar$ or $^{17}\Delta$ was observed over the cruise. Duplicate precision from either the underway or cast samples was similar to that for paired cast and underway samples (standard deviation 0.2% $\Delta O_2/Ar$ and 5 per meg in $^{17}\Delta$, n = 14 pairs). $^{17}\Delta$ in underway samples from 18 and 25 April (2.7°S and 3.5°N) was highly elevated compared to cast samples, but based on similar line and surface water temperatures and $\Delta O_2/Ar$, we conclude that degassing or air contamination were unlikely; these samples may reflect the influence of fine-scale environmental heterogeneity.

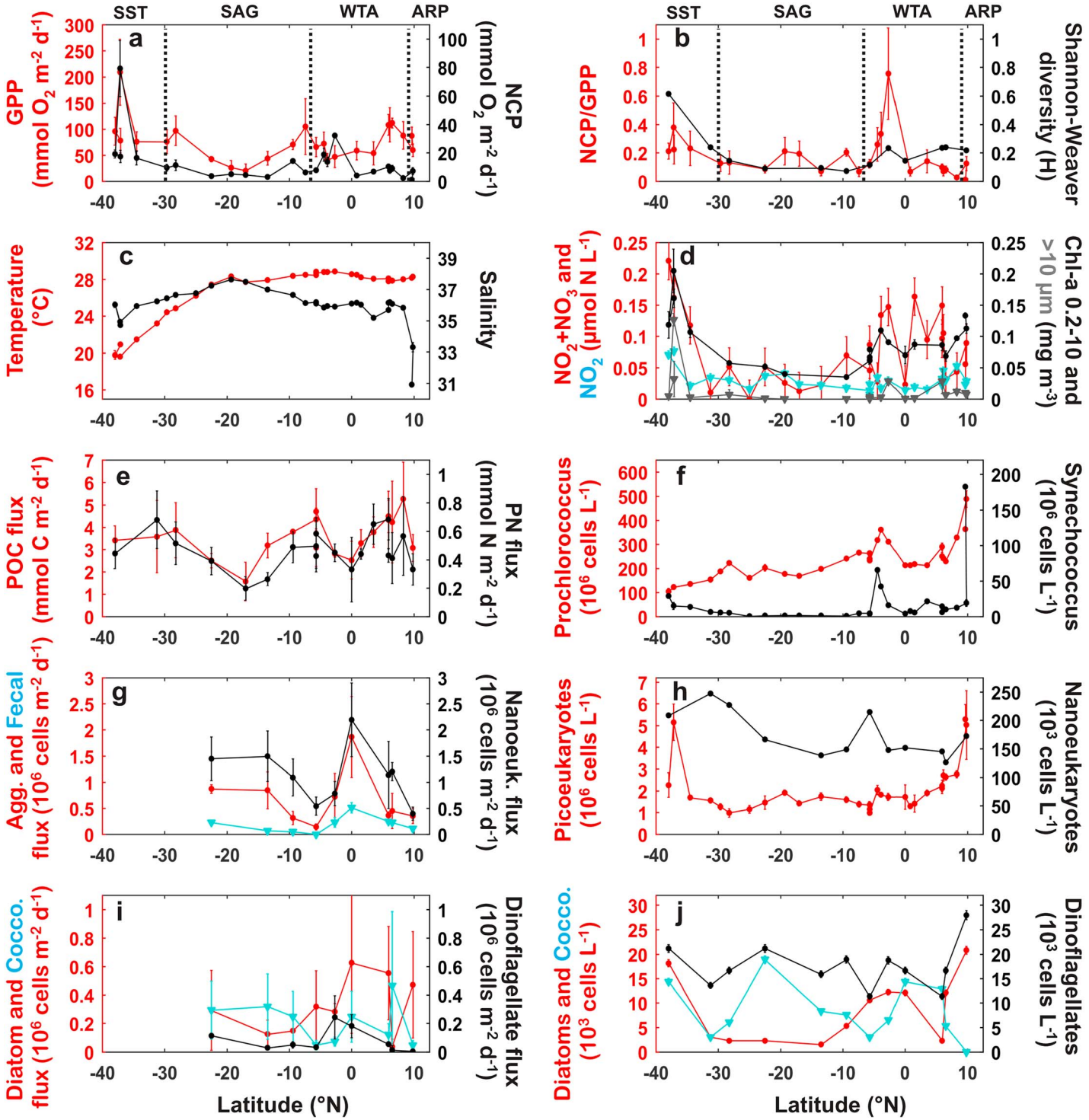

Figure 3. Measured and calculated parameters plotted against latitude. Biogeographic provinces are noted with dashed lines and abbreviations as in Figure 1. Throughout, the first variable on the left axis is marked by red filled circles and the second marked by cyan triangles, and the first variable on the right axis is marked by black circles and the second by gray triangles (axis labels colored similarly). Top row: (a) gross primary production (GPP) and net community production (NCP); and (b) the NCP/GPP ratio and Shannon-Weaver diversity (*H*) phytoplankton community. Second row: (c) temperature and salinity; and (d) total nitrite plus nitrate, nitrite only, and chlorophyll *a* concentrations for the 0.2–10 µm and >10 µm size fractions. Left-hand column from third row down: particle fluxes at 125 m, including (e) particulate organic carbon (POC) and particulate nitrogen (PN) fluxes; (g) cell aggregate, fecal pellet, and nanoeukaryote number fluxes; and (i) diatom, coccolithophore, and dinoflagellate number fluxes. Right hand column from third row down: abundances of (f) *Prochlorococcus* and *Synechococcus*; (h) picoeukaryotes and nanoeukaryotes, and (j) diatoms, coccolithophores, and dinoflagellates. Standard deviations are plotted as error bars (or are smaller than the marker size) on all variables except Shannon-Weaver diversity (*H*), which is a lower bound (see section 3.3 and Table S3).

3.1.2. Rates of Net Community Production and Gross Primary Production

Net community production and gross primary production in the surface mixed layer (Figures 1 and 3a) were high in the SST, with generally low to moderate values along the rest of the transect (NCP ~5 to 15 mmol O_2 m^{-2} d^{-1}, GPP ~40 to 100 mmol O_2 m^{-2} d^{-1} in general). NCP and GPP had, on average, standard deviations of 3 and 22 mmol O_2 m^{-1} d^{-1} (25% and 30%), respectively. Two outlier values of GPP reported in Table S2 (one sample each from the duplicate pairs at 19.3°S and 17.0°S) were excluded from the mean rates (see supporting information Text S3). Uncertainties for these duplicate pairs are still included in the reported rate precision.

The NCP/GPP ratio (Figure 3b) was between 0.1 and 0.2 across most of the transect; i.e., 10–20% of photosynthetic oxygen in the surface mixed layer was likely offset by organic matter export below the pycnocline or laterally advected over the residence time of oxygen in the mixed layer. The relative uniformity in NCP and GPP across the basin was punctuated by large variations between individual locations separated by hundreds of kilometers, leading to particularly pronounced changes to NCP/GPP (e.g., at 37.2°S and 2.7°S).

3.2. Nitrate, Nitrite, and Chlorophyll *a* Concentrations

The total nitrate and nitrite concentrations (Figure 3d) were higher in the SST and WTA (0.05 to 0.20 μmol N L^{-1}) than in the other regions. Nitrite concentrations were low across the subtropics and tropics (typically less than 0.05 μmol N L^{-1}). The nitrite and total nitrate plus nitrite duplicate precisions were 0.006 and 0.03 μmol N L^{-1}, respectively (precision of all samples at a location was similar). One measurement each of total nitrite plus nitrate from the filtered and unfiltered nutrient data sets was discarded (different locations) because they were more than two standard deviations higher than their duplicates and all other samples.

Peak values of chlorophyll *a* (Figure 3d) were found in the SST both for the 0.2 to 10 μm and >10 μm size fractions (>0.1 mg m^{-3} each). Values in the >10 μm fraction (likely associated with larger cells) were low (<0.03 mg m^{-3}) or below detection across the rest of the transect, while the 0.2 to 10 μm fraction was lowest in the SAG (~0.05 mg m^{-3}). Replicate precision was 9% (0.2 to 10 μm) and in the case of the >10 μm fraction generally varied between 10% and 100% (relative uncertainties were large at low concentrations).

3.3. Phytoplankton Abundance and Diversity

Picophytoplankton (Figures 3f and 3h) and nanophytoplankton and microphytoplankton (Figures 3h and 3j) abundances were previously presented in *Hennon* [2015] and *Durkin et al.* [2016]. Cyanobacteria (*Prochlorococcus* and *Synechococcus*) and picoeukaryotes (~10^8, 10^7, and 10^6 cells L^{-1}, respectively) were orders of magnitude more abundant than larger nanoeukaryotes and microeukaryotes such as diatoms (~10^5 and 10^3 to 10^4 cell L^{-1}, respectively). Picoeukaryotes followed a broadly similar trend to GPP. Abundances of cyanobacteria, nanoeukaryotes, diatoms, and coccolithophores all peaked locally in the equatorial region near similar features in NCP, GPP, NCP/GPP, and chlorophyll *a*. Uncertainties in cell abundance for each cell type were similar (on average, relative standard deviations of 3–13% for cell types measured by flow cytometry and 1–8% for light microscopy).

Shannon-Weaver diversity (Figure 3b) was low across the transect, reflecting the numerical dominance of *Prochlorococcus*. Diversity was highest in the SST where the lowest abundance of *Prochlorococcus* and highest abundances of nano-sized and microphytoplankton were observed. Community diversity was low throughout the SAG and slightly higher in the WTA and ARP due to higher abundances of larger phytoplankton. Rarefaction curves (Figure S3) indicate that microscopy sampling was insufficient to detect all phytoplankton morphotypes likely to be present within the mixed layer—thus, diversity may be underrepresented to different degrees across the transect and reported *H* is likely a lower bound.

3.4. Particle Fluxes

Fluxes at 125 m of POC and PN, as well as number fluxes of individual nano-size and microeukaryote phytoplankton, and number fluxes of cell aggregates and fecal pellets (Figures 3e, 3g, and 3i) have been previously reported in *Durkin et al.* [2016]. Particle number fluxes were more variable in the WTA than in the SAG. Particle number fluxes were not measured in the SST. These fluxes did not generally covary with production fluxes. Cell and particle type number fluxes had relative standard deviations of 30–60% on average.

Table 1. Production Rate Comparisons to Literature Values

Biogeographic Province	GPP mmol O_2 m^{-2} d^{-1} (SD)	NCP mmol O_2 m^{-2} d^{-1} (SD)	Methods	Time of Year	Reference
SST	115 (64)	33 (31)	O_2/Ar, TOI	Mar–May	this study
	130 (70)	66 (68)	O_2 bottle	May/Oct	*Serret et al.* [2015][a]
	98(26)		6 h ^{14}C-NPP	May/Oct	*Tilstone et al.* [2009][b]
		50 (16)	Satellite	Mar–May	*Tilstone et al.* [2015][c]
SAG	60 (32)	7 (4)	O_2/Ar, TOI	Mar–May	this study
	58 (4)	10 (2)	O_2 bottle	May/Oct	*Serret et al.* [2015][a]
	47 (4)		6 h ^{14}C-NPP	May/Oct	*Tilstone et al.* [2009][b]
	38 (18)		6 h ^{14}C-NPP	May/Oct	*Marañón et al.* [2003][d]
		−8 (2)	Satellite	Mar–May	*Tilstone et al.* [2009][c]
		4 (2)	Satellite	Mar–May	*Tilstone et al.* [2015][e]
WTA	75 (27)	11 (9)	O_2/Ar, TOI	Mar–May	this study
	100 (40)	28 (38)	O_2 bottle	May/Oct	*Serret et al.* [2015][a]
	58 (11)		6 h ^{14}C-NPP	May/Oct	*Tilstone et al.* [2009][b]
	152 (25)	15 (6)	O_2/Ar, TOI	May–June	*Yeung et al.* [2012]
		9 (4)	DIC	May–June	*Yeung et al.* [2012][f]
		11 (5)	Satellite	Mar–May	*Tilstone et al.* [2015][c]
ARP	73 (19)	4 (4)	O_2/Ar, TOI	Mar–May	this study
	206 (39)	78 (6)	O_2/Ar, TOI	May–June	*Yeung et al.* [2012]
		23 (7)	DIC	May–June	*Yeung et al.* [2012][f]

[a]Estimated from subset of reported euphotic zone integrated rates over similar locations as this study, May and October average.
[b]Six-hour radiocarbon incubation during morning modeled to 12 h average using daily light, converted assuming GPP(O)/NPP(C) = 2.7.
[c]Austral fall NCP over equivalent biogeographic province, using NCP_D definition from *Tilstone et al.* [2015].
[d]Six-hour radiocarbon incubation during afternoon assumed constant throughout sunlit hours, converted assuming GPP(O)/NPP(C) = 2.7.
[e]Austral fall NCP over equivalent biogeographic province, using NCP_C definition from *Tilstone et al.* [2015].
[f]Converted to oxygen units following assumptions of authors that O_2/C = 1.1 for diazotroph fueled growth.

While POC and PN fluxes were broadly similar throughout the transect (generally 2 to 5 mmol C m^{-2} d^{-1} and 0.2 to 0.7 mmol N m^{-2} d^{-1}), there was variability on the scale of hundreds of kilometers, similar to the gas tracer based production rates. In particular, POC flux followed a similar pattern as GPP. Average POC and PN flux standard deviations were 0.8 mmol C m^{-2} d^{-1} (24%) and 0.1 mmol N m^{-2} d^{-1} (28%), respectively, similar to the relative standard deviations of NCP and GPP.

4. Comparison of Production Rates With Literature Values

4.1. Net Community Production and Gross Primary Production

Rates of net community production and gross primary production presented in this work were compared with other published studies in the South Atlantic (Table 1). Other methods used to calculate primary production in this region included one study in the ARP also using the O_2/Ar and triple oxygen isotope tracers as well as dissolved inorganic carbon drawdown [*Yeung et al.*, 2012] and multiple years of coverage across the basin in May and October as part of the Atlantic Meridional Transect program [*Robinson et al.*, 2006, 2009], using euphotic zone integrated rates of radiocarbon uptake into particles [*Marañón et al.*, 2003; *Tilstone et al.*, 2009] and oxygen light-dark bottle incubations [*Serret et al.*, 2015]. We additionally compared our results to satellite-derived estimates of NCP based on satellite POC estimates and POC to NCP and temperature relationships derived from the AMT incubations [*Tilstone et al.*, 2015], which provided expanded spatial and temporal coverage. All rates were converted to oxygen fluxes for comparison (section 2.2.2).

In general, similar results were observed using different techniques over several years. GPP and NCP rates in the SST, SAG, and WTA agreed within standard deviations between this study (late March to early May) and the pooled incubation data (May and October). Higher NCP in the transition region compared to the subtropical gyre was consistent with results in other frontal regions [*Juranek et al.*, 2012; *Ostle et al.*, 2015; *Palevsky et al.*, 2013] and may have been related to enhanced nutrient supply from the subpolar gyre [*Ayers and Lozier*, 2010; *Palter et al.*, 2013]. Notably, both NCP and GPP rates in the SST had increased variability compared to other regions in this and the other studies; in particular, infrequent but high GPP and NCP features were

separated from regionally typical values over distances of ~100 km in both data sets. This agreement between data sets widely separated in time suggests that high variability and associated higher production rates may be persistent regional characteristics on top of basin-scale homogeneity.

Unlike the in situ results, the satellite-derived NCP indicated that the SAG was heterotrophic. The relationships used to derive NCP from satellite observations used pooled North and South Atlantic incubation data [*Tilstone et al.*, 2015]; much of the calibration data set was from the eastern North Atlantic subtropical gyre, where incubations were heterotrophic. However, the eastern North Atlantic may not be a good proxy for relationships between NCP and remotely sensed variables in the western SAG. An alternative satellite algorithm with no temperature dependence [*Tilstone et al.*, 2015] gave equivalently good fit to the calibration data in the SAG but resulted in autotrophic NCP rates that agree well with our estimate.

Mean production rates estimated from the two mesohaline ARP locations in this study (early May 2013) were significantly smaller (three times smaller GPP and 20 times smaller NCP) than rates at two mesohaline locations reported by *Yeung et al.* [2012] (May–June 2010), despite similar methods, gas exchange, and mixed layer depth. The higher production rates in *Yeung et al.* [2012] were likely caused by recurring, but transient, blooms of diatom-diazotroph associations that were not observed in our study. During this study, the diatom community was primarily composed of *Coscinodiscus*, *Pseudo-nitzschia*, *Cylindrotheca*, and *Nitzschia*, not the diazotroph-harboring *Hemiaulus* or *Rhizosolenia*. NCP rates from locations sampled by *Yeung et al.* [2012] in the WTA (rather than inside the Amazon River plume) were in agreement with the rates measured in this study.

4.2. Metabolic and Export Efficiency

The NCP/GPP ratio was generally between 0.1 and 0.2, similar to ratios observed in most studies to date [*Juranek and Quay*, 2013 and references therein]. On the basis of physiological studies [*Behrenfeld et al.*, 2008; *Halsey et al.*, 2010], a NCP/GPP ratio of approximately 0.4 may be a theoretical maximum [*Juranek and Quay*, 2013]. A NCP/GPP ratio of 0.4 is equivalent to a carbon-based NCP/NPP of roughly 0.8 (section 2.2.2). High NCP/GPP and *e*-ratios (POC flux/NPP; 0.7–0.8 in carbon units) have been observed in the subpolar North Atlantic during the spring bloom [*Buesseler*, 1998; *Quay et al.*, 2012] and the Bering Sea [*Prokopenko et al.*, 2011]. Two locations in this study had ratios near or exceeding an NCP/GPP ratio of 0.4.

The first location at 37.2°S (SST) had NCP/GPP = 0.38 (standard deviation 0.17; carbon based NCP/NPP = 0.73), in addition to the highest GPP and NCP fluxes and highest chlorophyll *a* concentrations in both size fractions of the transect, as well as low temperature and salinity compared to nearby locations. These unusual characteristics may have been related to eddy processes in the Brazil-Malvinas confluence region [e.g., *Gaube et al.*, 2014]. NCP/GPP from the second location (WTA, 2.7°S) was implausibly high (0.76, standard deviation 0.32), equivalent to carbon-based NCP/NPP = 1.45, which implies net carbon fixation in excess of local production. This high export ratio was because of the combination of moderate NCP and low GPP, and the uncertainties in the ratio were large. The mixed layer values could not be explained by enhanced vertical mixing (which would have led to a lower ratio in the surface; Figure 2). Similarly, the NCP/GPP peak was probably not explained by an increase in particle export efficiency as the export turnover rates of phytoplankton were moderate compared to elsewhere in the SAG and WTA [*Durkin et al.*, 2016].

This unusually elevated NCP/GPP was likely a result of temporal and spatial variability of NCP and GPP, such as has been observed in Lagrangian experiments [*Hamme et al.*, 2012]. Rapid changes in the balance of production and respiration add uncertainty to estimates of both NCP and GPP, potentially making the corresponding NCP/GPP less representative of average conditions. A potential driver for such changes is illustrated by the adjacent feature at 3.9°S, characterized by higher cyanobacterial abundance and chlorophyll *a* concentrations in both size fractions than other nearby locations. While surface abundance and export fluxes of larger phytoplankton were not sampled at this location, abundant *Rhizosolenia* were identified in surface water, a genus that blooms [*Murray et al.*, 1994; *Carpenter et al.*, 1999] or accumulates along surface frontal systems [*Yoder et al.*, 1994; *Kemp et al.*, 2006; *Wilson et al.*, 2008] and may host symbiotic diazotrophs [*Zehr et al.*, 2000; *Foster et al.*, 2009]. Similarly high ratios (NCP/GPP = 0.47, carbon-based NCP/NPP = 1.15 with $O_2/C = 1.1$) were determined in such a diatom-diazotroph association bloom in the mesohaline front of the Amazon River plume in 2010 [*Yeung et al.*, 2012]. It is possible that at

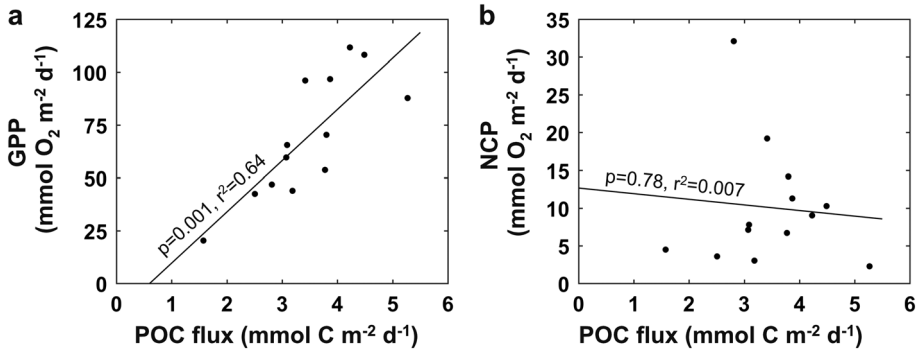

Figure 4. Correlations of particulate organic carbon (POC) flux at 125 m with (a) gross primary production (GPP) and (b) net community production (NCP) in the surface mixed layer across the transect. GPP significantly correlates with POC flux across the transect (*p* scores are for *F* test of regression significance), but NCP does not.

2.7°S the transitory presence of conditions similar to those observed at 3.9°S influenced our measured production rates.

5. Relationships Between Phytoplankton Community, Production, and Export

A notable feature of the results presented here is the basin-scale homogeneity of rates of biological production over thousands of kilometers in the subtropical and tropical Atlantic, despite variability over hundreds of kilometers. The gas-tracer derived measure of export was also relatively homogenous over the entire transect, consistent with POC export over the same region [*Owens et al.*, 2015; *Durkin et al.*, 2016], but was variable over the same length scales as the production rates. Indeed, many of the biological parameters measured in this study had qualitatively similar trends and variability to the oxygen-based production fluxes and export efficiency (Figure 3). This similarity in the patterns of production and biological properties may point to a common factor underlying the observed variability.

One mechanism by which the patterns of variability observed in this data set could arise is the mixing of biomass and nutrients on the mesoscale (tens to hundreds of kilometers) [*McGillicuddy et al.*, 2007; *Klein and Lapeyre*, 2009] and submesoscale (less than 10 km) [*Lévy et al.*, 2012; *Estapa et al.*, 2015; *Mahadevan*, 2016]. These mixing processes may exert control over the biological carbon pump by driving transient production and export pulses such as those described at the ocean time series [*Sweeney et al.*, 2003; *Nicholson et al.*, 2008; *Giesbrecht et al.*, 2012]. For example, high variability of POC export in the SST compared to other South Atlantic regions was previously ascribed to episodic nutrient addition by mesoscale features [*Thomalla et al.*, 2006], and mesoscale eddies on subtropical gyre boundaries may be associated with enhanced nutrient supply and community diversity [*McGillicuddy*, 2016]. Similarly, mixing and dispersion enhanced modeled phytoplankton community diversity at the mesoscale while homogenizing diversity across larger regions [*Lévy et al.*, 2014, 2015; *Clayton et al.*, 2013].

Despite similar patterns, different properties did not necessarily correlate well at each location. For example, while net community production, total cyanobacterial abundance, chlorophyll *a* concentrations (0.2 to 10 μm), and particle fluxes all had visually similar peaks in the equatorial region, the highest values of each property were separated by up to 5° of latitude. Thus, there were a limited number of significant correlations across the transect (Table S4). Interestingly, mean POC fluxes significantly correlated with GPP across the transect, but not with NCP (Figure 4).

The correlation between POC (and PN) fluxes and GPP, but not NCP, is somewhat unexpected. Conceptually, NCP should be balanced by export production over sufficient scales of time and space [*Emerson et al.*, 1997]. Particulate carbon flux is often assumed to dominate carbon export [*Michaels and Silver*, 1988; *Estapa et al.*, 2015]. Disagreement between particle export and oxygen-based NCP has been observed previously [*Steinberg et al.*, 2001; *Martz et al.*, 2008], potentially because of methodological biases in each technique [*Gardner*, 2000; *Buesseler et al.*, 2007, 2008; *Martz et al.*, 2008]. In particular, depth-dependent biases act differently on gas and trap based methods. Below we first discuss issues that might complicate the comparison of

NCP, GPP, and POC export fluxes and then the potential ecological meaning of the correlation between POC flux and GPP, but not NCP.

5.1. Interpreting Production and Export Over Multiple Scales of Space and Time

In general, the measures of community structure, production, and export that are evaluated in this work varied more in time or in space (over the typical sample resolution of 100 km or more) than the analytical uncertainties in the measurements (Tables S2 and S3). However, the dissolved gas tracers and particle export traps integrated across different scales of space (both horizontal and vertical) and time and thus may have been more or less sensitive to different processes.

The dissolved gas tracers are generally expected to integrate over a few days to 2 weeks and tens of kilometers based on their residence time with respect to gas exchange. However, we note that these tracers varied substantially over the timescale of hours (section 2.2.1 and supporting information Text S2; our sampling plan likely avoided systematic bias across the transect from diel patterns). These tracers may be more sensitive to short-term biological variability than was believed a decade ago [*Ferrón et al.*, 2015]. POC flux was less frequently evaluated across the transect than the gas tracers, and in general such rates integrate export processes over a few days or less and over a few kilometers of the surface ocean, but the surface origin of particles may be up to 10 km distant from the trap location [*Siegel et al.*, 2008]. Additionally, surface production and export may be spatially decoupled over scales of 10 to 100 km [*Plattner et al.*, 2005]. For example, recent work in the subtropical North Atlantic [*Estapa et al.*, 2015] found that on submesoscales (10 km or less), particulate export and NCP were decoupled, but when integrating over several measurements throughout a mesoscale transect (order of 30 km), the two fluxes agreed in magnitude. Thus, the gas tracer derived rates and POC export should be compared with caution at any single location. Despite these issues, the relative homogeneity of the production and export rates across thousands of kilometers may indicate that such considerations do not greatly bias the transect-wide comparison.

Another source of uncertainty in comparing these rates is their different sensitivities to depth-dependent processes. Without longer time series in the subsurface, the gas tracers can be used to evaluate only surface mixed layer production; production within the euphotic zone but below the mixed layer is not accounted for. However, it is likely that mixed layer production captured $>$70% of GPP in the WTA and ARP and $>$90% in the SST and SAG, based on available productivity depth profiles from the tropical and subtropical South Atlantic (from radiocarbon; *Poulton et al.* [2006]) and from comparable seasonal observations and model results at the Bermuda Atlantic Time Series (from radiocarbon and triple oxygen isotopes; *Nicholson et al.* [2012]). This conclusion is supported by observations of euphotic zone depth (the depth to which 1% of incident surface PAR flux penetrates), across the transect (Table S3); in most cases $<$15% of the cumulative photosynthetically active radiation (PAR) flux integrated across the euphotic zone penetrates below the mixed layer. In the ARP 50% of integrated PAR flux could have penetrated below the mixed layer defined after *Levitus* [1982], but the surface density gradient was unusually large because of the plume's low-salinity lens—inspection of the density profile indicates an 80 m mixed layer depth, implying that the euphotic zone was entirely within the mixed layer. The four stations in the WTA with very shallow reported mixed layer depths similarly may have had deeper mixed layers (40–45 m) based on inspection of density profiles, and the surface rates may have represented a greater portion of euphotic zone production.

Similarly, NCP in the surface mixed layer did not account for changes in community metabolism with depth, but in general, $\Delta O_2/Ar$ below the mixed layer and within the euphotic zone ranged from near zero to greater than that in the surface (Figure 2). Therefore, production generally balanced or exceeded respiration throughout the euphotic zone. If production rates below the mixed layer were low (above), respiration rates at these depths must have been similarly low (i.e., no greater than production; otherwise; $\Delta O_2/Ar$ would be negative). Thus, surface mixed layer NCP may have underestimated total euphotic zone NCP but likely accounted for a similar fraction of the total as for GPP, i.e., $>$70–90%. $\Delta O_2/Ar$ was only negative within the deeper euphotic zone from 2.7°S to 3.9°S; based on the hydrography, this signal likely indicated shoaling of deeper waters (Figure 2) rather than local respiration associated with in situ production (POC flux was still uncorrelated with NCP if these data were removed, $p = 0.28$).

In contrast, particle export at 125 m depth encompassed processes occurring throughout much or all of the euphotic zone and may have also included particle attenuation from respiration below the euphotic

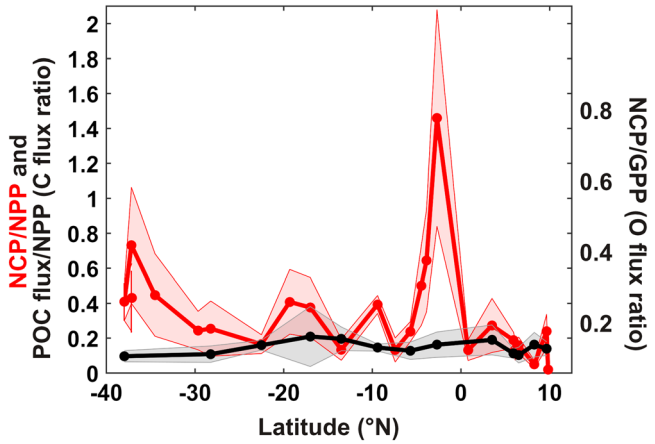

Figure 5. Export ratio estimates from O_2/Ar-based net community production (NCP) and particulate organic carbon (POC) flux, relative to net primary production (NPP; scaled from triple oxygen isotope based gross primary production, GPP). NCP/NPP export ratio and standard deviation (red), and the POC flux/NPP export ratio and standard deviation (black) are plotted in carbon units on the left-hand axis and oxygen units (relative to GPP rather than NPP) on the right-hand axis. NCP/NPP peaks at 37.2°S and 2.9°S are discussed in the text.

zone [*Martin et al.*, 1987]. In general, differences in POC flux across the transect were small compared to changes in GPP and NCP, and we do not expect the behavior of the two production fluxes to have differed with respect to POC flux without some environmentally meaningful process such as particle loss with depth or export of carbon through nonparticle pathways.

5.2. Ecological Links Between Production Rates and Particulate and Dissolved Organic Carbon Export

NCP and POC flux did not correlate across the transect. Mismatches could reflect both methodological issues in the comparison and inadequate spatial resolution of the comparisons; however, we argue above that these biases should have been small compared to the measured rates. Furthermore, GPP should in general have been affected by the same potential biases as NCP and to a similar degree, and yet, GPP and POC flux were significantly correlated.

Thus, the difference between NCP and POC fluxes likely reflected real ecosystem processes, such as respiration of sinking particles below the mixed layer, or a large contribution of dissolved organic carbon or zooplankton mediated fluxes to carbon export. Carbon produced in the mixed layer and ultimately lost from the surface by either of these two latter processes was reflected in gas tracer based estimates of NCP, but not in the particle flux. It has been observed that a sizable fraction of NCP can be funneled into DOC export or storage with some community structures [*Emerson*, 2014; *Ducklow et al.*, 2015], and some DOC production and export may be mediated by microbial cleaving and consumption of POC [*Jiao et al.*, 2010; *Buchan et al.*, 2014; *Mislan et al.*, 2014]. Vertically migrating zooplankton may consume surface-derived POC and produce fecal pellets, respire, or excrete DOC at depth, with associated carbon fluxes from 0% to 39% as large as the POC flux in equatorial and subtropical regions [*Zhang and Dam*, 1997; *Steinberg et al.*, 2000; *Al-Mutairi and Landry*, 2001].

We compare export ratios of NCP and POC flux using NCP/GPP in order to evaluate the potential role of DOC or zooplankton mediated fluxes in balancing organic matter production. NCP and GPP are converted to carbon-based units as described in section 2.2.2. NCP and the gas tracer implied export ratio were both more variable and generally greater than the POC flux and export ratio (Figure 5). Comparing only locations where both NCP and POC export fluxes were evaluated, POC flux at 125 m accounted for 82% of total NCP across the transect (standard deviation 81%, 95% confidence interval of 38% to 126%). The mean value was not well constrained, reflecting the variability of NCP, the potential variability of DOC fluxes and POC respiration, and low sample resolution. Nonetheless, the difference could be interpreted as equivalent to DOC storage or export accounting for 18% of NCP, in agreement with estimates that DOC accounts for 17% of euphotic zone NCP in the Atlantic [*Romera-Castillo et al.*, 2016] and ~20% of export to below 130 m globally [*Hansell*, 2013]. This relationship was equivalent but slightly better constrained in the South Atlantic gyre, with 76% of NCP potentially accounted for by POC export (standard deviation 46%, n = 5). Observations are more sparse in the South Atlantic than in the North Atlantic, but modeled annual DOC fluxes are on the order of 1–2 mmol DOC m^{-2} d^{-1} in the western subtropical and tropical Atlantic [*Hansell et al.*, 2012] or ~25% of our measured NCP. Thus, the average difference between NCP and POC export could plausibly be explained by DOC fluxes in the subtropical and tropical regions.

Table 2. Region Differences in Property Median, Distribution, and Variance

Test[a] Variable	Kruskal-Wallis[b] (Median)	Anderson-Darling (Distribution)	Brown-Forsythe (Variance)
Gross primary production			all ≠, except SST ~ ARP
Net community production	SST > SAG	SST ≠ SAG, WTA, ARP	WTA ≠ SST, SAG, ARP; SAG ≠ ARP
NCP/GPP ratio		SST ≠ SAG, ARP	SAG ≠ WTA
$NO_3 + NO_2$		SAG ≠ WTA	SAG ≠ WTA
NO_2			SST ≠ SAG, WTA, SAG ≠ WTA
Chlorophyll *a* 0.2 to 10 μm	SAG < SST, ARP	all ≠, except SST ~ ARP	SST ≠ SAG, WTA, SAG ≠ WTA
Chlorophyll *a* >10 μm		SAG ≠ ARP	SST ≠ SAG, WTA, SAG ≠ WTA
Cyanobacteria	SST < WTA, ARP; SAG < ARP	all regions	all ≠, except SST ~ ARP
Picoeukaryotes	SAG < ARP	SST ≠ SAG; ARP ≠ SAG, WTA	ARP ≠ SST, WTA
Nanoscale and larger eukaryotes		SST ≠ SAG, WTA	SAG ≠ WTA
Shannon-Weaver diversity (*H*)	SST > SAG	SAG ≠ SST, WTA	SAG ≠ WTA
Nanoscale and larger flux			
Cell aggregate flux			
Fecal pellet flux			
Particulate organic carbon flux			SAG ≠ WTA
Particulate nitrogen flux			

[a]Nonparametric tests used, see section 2.6.
[b]With Dunn-Šidák correction for multiple comparisons.

The correlation between GPP and POC flux across the transect may provide a clue that particle export was directly linked to total photosynthetic production despite decoupling of NCP and POC fluxes as hypothesized above. This is consistent with recent findings that picophytoplankton can export carbon in proportion to their contribution to NPP (or proportionally GPP) in tropical and subtropical regions, possibly through cell aggregation and fecal packaging by zooplankton [*Richardson and Jackson*, 2007; *Stukel and Landry*, 2010; *Guidi et al.*, 2016]. While size-fractionated primary production was not measured, in situ growth rates of *Prochlorococcus* and *Synechococcus* in the surface waters (5 m) during this cruise could account for much of the observed surface mixed layer GPP across the transect [*Hennon*, 2015]. Similar proportions of total production (roughly 60% in the SAG and WTA) along a May 2004 transect in the same regions were attributed to picophytoplankton based on size-fractionated primary production [*Poulton et al.*, 2006]. Thus, the link between POC export and photosynthesis is potentially explained by the packaging and export of cyanobacteria-derived carbon.

5.3. Relationships With Respect to Community Structure and Biogeographic Provinces

The biogeographic provinces identified in section 2.5 are an ecologically meaningful way to bin the sample results in order to maximize data set overlap and minimize small-scale spatial and temporal offsets between data types. Significantly different ($p < 0.05$) regional medians, sample distributions, and variances are summarized in Table 2 (correlations of properties by province in Table S5). In general, the *variance and distribution* of observed values varied more between regions than the *means* or *medians* did. The most variable regions (for most measurements) were the SST and WTA, which skewed toward higher values of GPP, NCP, NCP/GPP ratio, and community diversity (Figure S4; though the limited number of locations in the SST may have led to larger apparent variability). This variability of biological production and community characteristics distinguished between regions that were otherwise similar in the mean sense [*Howard*, 2017] and may indicate that the observed biological fluxes were influenced by shared underlying mechanisms of variability.

In order to evaluate potential connections between surface phytoplankton communities and production measures, community structure associations were also identified (Figure S5). However, no clear link between community structure and production or export rates was observed in this data set; the phytoplankton community in the surface (5 m) did not necessarily reflect what sank below the mixed layer at the time of sampling, and locations with the same broad surface community structure did not necessarily share particle export mechanisms [*Durkin et al.*, 2016]. In particular, we did not observe expected relationships of GPP (or NPP) with diversity [e.g., *Napoléon et al.*, 2014] or increased particle export in community structures influenced by larger phytoplankton such as diatoms [*Michaels and Silver*, 1988]; the latter finding is consistent with that from a similar Southern Ocean data set [*Cassar et al.*, 2015]. The lack of correlations may be because the number of locations with concurrent productivity data was too few to detect significant differences or because the

surface community structure sampled at 5 m did not fully represent the portion of the overall euphotic zone community responsible for production and export over the space and time scales of our observations.

However, observed surface phytoplankton diversity across the South Atlantic was similar to patterns derived from self-assembling phytoplankton communities in global circulation and biogeochemistry models [*Barton et al.*, 2010; *Clayton et al.*, 2013; *Lévy et al.*, 2014, 2015]. These model results may indicate that mixing at both basin and mesoscales (thousands and tens to hundreds of kilometers respectively) and resulting effects on nutrient supply could help explain the diversity patterns we observed. Regional correlations between variance of surface diversity and nutrients ($p = 0.02$ with nitrite and $p = 0.03$ with nitrate plus nitrite) were observed, as were basin-scale correlations between diversity and nitrite and total nitrate plus nitrite concentrations ($p = 1 \times 10^{-4}$, $p = 0.008$) and *Synechococcus* abundance ($p = 7 \times 10^{-5}$). While nutrient supply was not evaluated, these findings may indicate that changes in the availability of inorganic nitrogen play a key role in allowing other phytoplankton to better compete for this primary limiting nutrient relative to the numerically dominant *Prochlorococcus*; most identified isolates of *Prochlorococcus* grow only on ammonia, though some strains have recently been discovered to assimilate nitrite and nitrate [*Moore et al.*, 2002; *Martiny et al.*, 2009, *Berube et al.*, 2015].

6. Conclusion

We used a suite of in situ measurements of community structure, biological production, and particulate export to evaluate how fluxes associated with the biological carbon pump varied meridionally across the equatorial and South Atlantic Ocean in austral fall of 2013. This work highlights the basin-scale homogeneity of rates of biological production and carbon export over the transect, but variability was observed over hundreds of kilometers.

POC and PN export correlated with GPP, suggesting that there may be a link between photosynthesis and ultimate particle export when picophytoplankton are most abundant in the surface and potentially account for much of the observed surface production. This finding is consistent with the hypothesis of *Richardson and Jackson* [2007] that picoplankton contribute to export in proportion to their contribution to community autotrophic production, regardless of the expected slow sinking rates of individual small cells. At the same time, the lack of correlation between NCP and POC export may indicate the importance of dissolved organic carbon or zooplankton mediated fluxes to export; quantitatively, the relative magnitude of POC to NCP fluxes implies a DOC export rate consistent with both global and regional estimates of the contribution of DOC to carbon export from the surface mixed layer.

While we did not observe significant differences in carbon cycling between different surface community structure types or in the mean sense between biogeographic regions, there were differences in the variability of biological production and community characteristics between regions. Phytoplankton community diversity and nutrient concentrations may have been linked, and observed diversity was similar to patterns predicted in global models based on mixing of nutrients over various spatial scales.

Additional specific findings of interest include the following:

1. Production rates based on in situ biogeochemical tracers (this study) and other methods were generally in agreement [*Marañón et al.*, 2003; *Tilstone et al.*, 2009; *Serret et al.*, 2015].
2. Disagreement between production rates measured at the mesohaline edge of the Amazon River plume in early May 2013 (this study) with those from May–June 2010 [*Yeung et al.*, 2012] using nearly identical methods points to the dynamic nature of this environment and potentially to the influence of blooms by diatom-diazotroph associations on production.
3. Some common assumptions in the calculation of gross primary production and net community production from oxygen based tracers may introduce additional errors to rate estimates. In particular, results may be sensitive to the time of sampling because diel cycles may be large relative to average tracer values.

Acknowledgments

Cruise KN201-04 was supported by NSF grant OCE 1154320 to E.B. Kujawinski and K. Longnecker (WHOI). E.M.H. was supported by grants from the WHOI Ocean and Climate Change Institute and WHOI Ocean Life Institute to R.H.R. S., and the National Defense Science and Engineering Graduate Fellowship program. C.A.D. was supported by the WHOI Devonshire Postdoctoral Scholarship. G.M.M.H. and F.R. were supported by Gordon and Betty Moore Foundation grant 537.01 to E.V. Armbrust (UW). R.H.R.S. was supported by NSF grant OCE 1029676. We would like to thank the captain, crew, and shipboard scientific technicians of the R/V *Knorr* for at sea support, and cruise principal investigators E.B. Kujawinski and K. Longnecker for inviting participation on KN201-04 and generous in-kind support. We also thank E.V. Armbrust for supporting the work of G. M.M.H. and F.R. on this project. We are grateful to Z. Sandwith for cruise setup and laboratory assistance with gas tracer analyses and J. Swallwell for assistance with setup and operation of the SeaFlow continuous underway flow cytometry system and to B. Van Mooy and J. Ossolinski for support in collecting sediment trap samples. We also thank A.E. Giblin, A.C. Spivak, and the anonymous reviewers for comments that greatly improved this manuscript. The authors do not have any real or perceived conflicts of interest due to finances or affiliations. Supporting data are included as tables in the supporting information files, along with supporting text and figures. Additional hydrographic data are available through BCO-DMO (http://www.bco-dmo.org/project/2204). All other data used are cited and referred to in the reference list.

References

Abe, O., and N. Yoshida (2003), Partial pressure dependency of $^{17}O/^{16}O$ and $^{18}O/^{16}O$ of molecular oxygen in the mass spectrometer, *Rapid Commun. Mass Spectrom.*, *17*(5), 395–400, doi:10.1002/rcm.923.

Acker, J. G., and G. Leptoukh (2007), Online analysis enhances use of NASA Earth Science Data, *Eos Trans. AGU*, *88*(2), 14, doi:10.1029/2007EO020003.

Al-Mutairi, H., and M. R. Landry (2001), Active export of carbon and nitrogen at Station ALOHA by diel migrant zooplankton, *Deep Sea Res., Part II*, *48*(8), 2083–2103, doi:10.1016/S0967-0645(00)00174-0.

Angert, A., S. Rachmilevitch, E. Barkan, and B. Luz (2003), Effects of photorespiration, the cytochrome pathway, and the alternative pathway on the triple isotopic composition of atmospheric O_2, *Global Biogeochem. Cycles*, *17*(1), 1030, doi:10.1029/2002GB001933.

Arar, E. J., and G. B. Collins (1997), *Method 445.0 in Vitro Determination of Chlorophyll a and Pheophytin in Marine and Freshwater Algae by Fluorescence*, Tech. Rep., 22, US Environmental Protection Agency, Washington, D. C.

Ayers, J. M., and M. S. Lozier (2010), Physical controls on the seasonal migration of the North Pacific transition zone chlorophyll front, *J. Geophys. Res.*, *115*, C05001, doi:10.1029/2009JC005596.

Ayers, J. M., and M. S. Lozier (2012), Unraveling dynamical controls on the North Pacific carbon sink, *J. Geophys. Res.*, *117*, C01017, doi:10.1029/2011JC007368.

Barkan, E., and B. Luz (2003), High-precision measurements of $^{17}O/^{16}O$ and $^{18}O/^{16}O$ of O_2 and O_2/Ar ratio in air, *Rapid Commun. Mass Spectrom.*, *17*(24), 2809–2814, doi:10.1002/rcm.1267.

Barton, A. D., S. Dutkiewicz, G. Flierl, J. Bragg, and M. J. Follows (2010), Patterns of diversity in marine phytoplankton, *Science*, *327*(5972), 1509–1511, doi:10.1126/science.1184961.

Behrenfeld, M. J., and P. G. Falkowski (1997), Photosynthetic rates derived from satellite-based chlorophyll concentration, *Limnol. Oceanogr.*, *42*(1), 1–20, doi:10.4319/lo.1997.42.1.0001.

Behrenfeld, M. J., K. H. Halsey, and A. J. Milligan (2008), Evolved physiological responses of phytoplankton to their integrated growth environment, *Philos. Trans. R. Soc. London, Ser. B*, *363*(1504), 2687–2703, doi:10.1098/rstb.2008.0019.

Benitez-Nelson, C., K. O. Buesseler, D. M. Karl, and J. Andrews (2001), A time-series study of particulate matter export in the North Pacific subtropical gyre based on ^{234}Th:^{238}U disequilibrium, *Deep Sea Res., Part I*, *48*(12), 2595–2611, doi:10.1016/S0967-0637(01)00032-2.

Berube, P. M., et al. (2015), Physiology and evolution of nitrate acquisition in *Prochlorococcus*, *ISME J.*, *9*(5), 1195–1207, doi:10.1038/ismej.2014.211.

Boyd, P., and P. Newton (1995), Evidence of the potential influence of planktonic community structure on the interannual variability of particulate organic carbon flux, *Deep Sea Res., Part I*, *42*(5), 619–639, doi:10.1016/0967-0637(95)00017-Z.

Boyd, P. W., and T. W. Trull (2007), Understanding the export of biogenic particles in oceanic waters: Is there consensus?, *Prog. Oceanogr.*, *72*(4), 276–312, doi:10.1016/j.pocean.2006.10.007.

Brandt, P., F. A. Schott, C. Provost, A. Kartavtseff, V. Hormann, B. Bourlès, and J. Fischer (2006), Circulation in the central equatorial Atlantic: Mean and intraseasonal to seasonal variability, *Geophys. Res. Lett.*, *33*, L07609, doi:10.1029/2005GL025498.

Brix, H., N. Gruber, D. M. Karl, and N. R. Bates (2006), On the relationships between primary, net community, and export production in subtropical gyres, *Deep Sea Res., Part II*, *53*(5), 698–717, doi:10.1016/j.dsr2.2006.01.024.

Brown, M. B., and A. B. Forsythe (1974), Robust tests for the equality of variances, *J. Am. Stat. Assoc.*, *69*(346), 364–367, doi:10.1080/01621459.1974.10482955.

Buchan, A., G. R. LeCleir, C. A. Gulvik, and J. M. Gonzalez (2014), Master recyclers: Feature and functions of bacteria associated with phytoplankton blooms, *Nature Rev. Microbio*, *12*, 686–698, doi:10.1038/nrmicro3326.

Buesseler, K. O. (1998), The decoupling of production and particulate export in the surface ocean, *Global Biogeochem. Cycles*, *12*(2), 297–310, doi:10.1029/97GB03366.

Buesseler, K. O., et al. (2007), An assessment of the use of sediment traps for estimating upper ocean particle fluxes, *J. Mar. Res.*, *65*(3), 345–416.

Buesseler, K. O., C. Lamborg, P. Cai, R. Escoube, R. Johnson, S. Pike, P. Masque, D. McGillicuddy, and E. Verdeny (2008), Particle fluxes associated with mesoscale eddies in the Sargasso Sea, *Deep Sea Res., Part II*, *55*(10), 1426–1444, doi:10.1016/j.dsr2.2008.02.007.

Carpenter, E., J. Montoya, J. Burns, M. Mulholland, A. Subramaniam, and D. Capone (1999), Extensive bloom of a N_2-fixing diatom/cyanobacterial association in the tropical Atlantic Ocean, *Mar. Ecol. Prog. Ser.*, *185*, 273–283, doi:10.3354/meps185273.

Carpenter, J. H. (1965a), The accuracy of the Winkler method for dissolved oxygen analysis, *Limnol. Oceanogr.*, *10*(1), 135–140, doi:10.4319/lo.1965.10.1.0135.

Carpenter, J. H. (1965b), The Chesapeake Bay Institute technique for the Winkler dissolved oxygen method, *Limnol. Oceanogr.*, *10*(1), 141–143, doi:10.4319/lo.1965.10.1.0141.

Carr, M.-E., N. S. Oakey, B. Jones, and M. R. Lewis (1992), Hydrographic patterns and vertical mixing in the equatorial Pacific along 150°W, *J. Geophys. Res.*, *97*(C1), 611–626, doi:10.1029/91JC02479.

Cassar, N., P. J. DiFiore, B. A. Barnett, M. L. Bender, A. R. Bowie, B. Tilbrook, K. Petrou, K. J. Westwood, S. W. Wright, and D. Lefevre (2011), The influence of iron and light on net community production in the Subantarctic and Polar Frontal Zones, *Biogeosciences*, *8*(2), 227–237, doi:10.5194/bg-8-227-2011.

Cassar, N., S. W. Wright, P. G. Thomson, T. W. Trull, K. J. Westwood, M. de Salas, A. Davidson, I. Pearce, D. M. Davies, and R. J. Matear (2015), The relation of mixed-layer net community production to phytoplankton community composition in the Southern Ocean, *Global Biogeochem. Cycles*, *29*, 446–462, doi:10.1002/2014GB004936.

Clayton, S., S. Dutkiewicz, O. Jahn, and M. J. Follows (2013), Dispersal, eddies, and the diversity of marine phytoplankton, *Limnol. Oceanogr. Fluids Environ.*, *3*, 182–197, doi:10.1215/21573689-2373515.

Clayton, S., T. Nagai, and M. J. Follows (2014), Fine scale phytoplankton community structure across the Kuroshio Front, *J. Plankton Res.*, *36*(4), 1017–1030, doi:10.1093/plankt/fbu020.

Craig, H., and T. Hayward (1987), Oxygen Supersaturation in the ocean: Biological versus physical contributions, *Science*, *235*(4785), 199–202, doi:10.1126/science.235.4785.199.

Dring, M. J., and D. H. Jewson (1982), What does ^{14}C uptake by phytoplankton really measure? A theoretical modelling approach, *Proc. R. Soc. B Biol. Sci.*, *214*(1196), 351–368, doi:10.1098/rspb.1982.0016.

Ducklow, H., D. Steinberg, and K. Buesseler (2001), Upper ocean carbon export and the biological pump, *Oceanography*, *14*(4), 50–58, doi:10.5670/oceanog.2001.06.

Ducklow, H. W., S. C. Doney, and S. F. Sailley (2015), Ecological controls on biogeochemical fluxes in the western Antarctic peninsula studied with an inverse foodweb model, *Adv. Polar Sci.*, 122–139, doi:10.13679/J.ADVPS.2015.2.00122.

Durkin, C. A., B. A. S. Van Mooy, S. T. Dyhrman, and K. O. Buesseler (2016), Sinking phytoplankton associated with carbon flux in the Atlantic Ocean, *Limnol. Oceanogr.*, *61*(4), 1172–1187, doi:10.1002/lno.10253.

Emerson, S. (2014), Annual net community production and the biological carbon flux in the ocean, *Global Biogeochem. Cycles*, *28*, 14–28, doi:10.1002/2013GB004680.

Emerson, S., P. D. Quay, C. Stump, D. Wilbur, and M. Knox (1991), O_2, Ar, N_2, and ^{222}Rn in surface waters of the subarctic ocean: Net biological O_2 production, *Global Biogeochem. Cycles*, *5*(1), 49–69, doi:10.1029/90GB02656.

Emerson, S., P. D. Quay, C. Stump, D. Wilbur, and R. Schudlich (1995), Chemical tracers of productivity and respiration in the subtropical Pacific Ocean, *J. Geophys. Res.*, *100*(C8), 15,873–15,887, doi:10.1029/95JC01333.
Emerson, S., P. Quay, D. Karl, C. Winn, L. Tupas, and M. Landry (1997), Experimental determination of the organic carbon flux from open-ocean surface waters, *Nature*, *389*(6654), 951–954, doi:10.1038/40111.
Emerson, S., T. Ito, and R. C. Hamme (2012), Argon supersaturation indicates low decadal-scale vertical mixing in the ocean thermocline, *Geophys. Res. Lett.*, *39*, L18610, doi:10.1029/2012GL053054.
Eppley, R. W., and B. J. Peterson (1979), Particulate organic matter flux and planktonic new production in the deep ocean, *Nature*, *282*(5740), 677–680, doi:10.1038/282677a0.
Estapa, M. L., D. A. Siegel, K. O. Buesseler, R. H. R. Stanley, M. W. Lomas, and N. B. Nelson (2015), Decoupling of net community and export production on submesoscales in the Sargasso Sea, *Global Biogeochem. Cycles*, *29*, 1266–1282, doi:10.1002/2014GB004913.
Falkowski, P. G., E. A. Laws, R. T. Barber, and J. W. Murray (2003), Phytoplankton and their role in primary, new, and export production, in *Ocean Biogeochemistry*, pp. 99–121, Springer, Berlin.
Ferrón, S., S. T. Wilson, S. Martínez-García, P. D. Quay, and D. M. Karl (2015), Metabolic balance in the mixed layer of the oligotrophic North Pacific Ocean from diel changes in O_2/Ar saturation ratios, *Geophys. Res. Lett.*, *42*, 3421–3430, doi:10.1002/2015GL063555.
Fisher, R. A. (1956), *Statistical Methods and Scientific Inference*, Hafner, Oxford, U. K.
Foster, R. A., A. Subramaniam, and J. P. Zehr (2009), Distribution and activity of diazotrophs in the eastern equatorial Atlantic, *Environ. Microbiol.*, *11*(4), 741–750, doi:10.1111/j.1462-2920.2008.01796.x.
Friedrichs, M. A. M., et al. (2009), Assessing the uncertainties of model estimates of primary productivity in the tropical Pacific Ocean, *J. Mar. Syst.*, *76*(1), 113–133, doi:10.1016/j.jmarsys.2008.05.010.
Garcia, H. E., and L. I. Gordon (1992), Oxygen solubility in seawater: Better fitting equations, *Limnol. Oceanogr.*, *37*(6), 1307–1312, doi:10.4319/lo.1992.37.6.1307.
Garcia, H. E., and L. I. Gordon (1993), Erratum: Oxygen solubility in seawater: Better fitting equations, *Limnol. Oceanogr.*, *38*(3), 656.
Gardner, W. D. (2000), Sediment trap sampling in surface waters, in *The Changing Ocean Carbon Cycle: A Midterm Synthesis of the Joint Global Ocean Flux Study*, edited by R. B. Hanson, H. W. Ducklow, and J. G. Field, pp. 240–284, Cambridge Univ. Press, Cambridge.
Gaube, P., D. J. McGillicuddy, D. B. Chelton, M. J. Behrenfeld, and P. G. Strutton (2014), Regional variations in the influence of mesoscale eddies on near-surface chlorophyll, *J. Geophys. Res. Oceans*, *119*, 8195–8220, doi:10.1002/2014JC010111.
Gehrie, E., D. Archer, S. Emerson, C. Stump, and C. Henning (2006), Subsurface ocean argon disequilibrium reveals the equatorial Pacific shadow zone, *Geophys. Res. Lett.*, *33*, L18608, doi:10.1029/2006GL026935.
Giesbrecht, K. E., R. C. Hamme, and S. R. Emerson (2012), Biological productivity along line P in the subarctic northeast Pacific: In situ versus incubation-based methods, *Global Biogeochem. Cycles*, *26*, GB3028, doi:10.1029/2012GB004349.
Gordon, L. I., J. C. Jennings, A. A. Ross, and J. M. Krest (1993), *A Suggested Protocol for Continuous Flow Automated Analysis of Seawater Nutrients (Phosphate, Nitrate, Nitrite and Silicic Acid) in the WOCE Hydrographic Program and the Joint Global Ocean Fluxes Study*, Tech. Rep., 55 pp., WOCE Hydrographic Program Office Methods Manual WHPO 91-1, Corvallis, Oreg.
Grodsky, S. A., J. A. Carton, and C. R. McClain (2008), Variability of upwelling and chlorophyll in the equatorial Atlantic, *Geophys. Res. Lett.*, *35*, L03610, doi:10.1029/2007GL032466.
Guidi, L., et al. (2016), Plankton networks driving carbon export in the oligotrophic ocean, *Nature*, *532*(7600), 465–470, doi:10.1038/nature16942.
Guidi, L., L. Stemmann, G. A. Jackson, F. Ibanez, H. Claustre, L. Legendre, M. Picheral, and G. Gorsky (2009), Effects of phytoplankton community on production, size, and export of large aggregates: A world-ocean analysis, *Limnol. Oceanogr.*, *54*(6), 1951–1963, doi:10.4319/lo.2009.54.6.1951.
Halsey, K. H., A. J. Milligan, and M. J. Behrenfeld (2010), Physiological optimization underlies growth rate-independent chlorophyll-specific gross and net primary production, *Photosynth. Res.*, *103*(2), 125–137, doi:10.1007/s11120-009-9526-z.
Hamme, R. C., et al. (2012), Dissolved O_2/Ar and other methods reveal rapid changes in productivity during a Lagrangian experiment in the Southern Ocean, *J. Geophys. Res.*, *117*, C00F12, doi:10.1029/2011JC007046.
Hamme, R. C., and S. R. Emerson (2004), The solubility of neon, nitrogen and argon in distilled water and seawater, *Deep Sea Res., Part I*, *51*(11), 1517–1528, doi:10.1016/j.dsr.2004.06.009.
Hansell, D. A. (2013), Recalcitrant dissolved organic carbon fractions, *Annu. Rev. Mar. Sci.*, *5*, 421–445, doi:10.1146/annurev-marine-120710-100757.
Hansell, D. A., C. A. Carlson, and R. Schlitzer (2012), Net removal of major marine dissolved organic carbon fractions in the subsurface ocean, *Global Biogeochem. Cycles*, *26*, GB1016, doi:10.1029/2011GB004069.
Hansell, D., C. A. Carlson, D. Repeta, and R. Schlitzer (2009), Dissolved organic matter in the ocean: A controversy stimulates new insights, *Oceanography*, *22*(4), 202–211, doi:10.5670/oceanog.2009.109.
Haskell, W. Z., D. Kadko, D. E. Hammond, A. N. Knapp, M. G. Prokopenko, W. M. Berelson, and D. G. Capone (2015), Upwelling velocity and eddy diffusivity from ^{7}Be measurements used to compare vertical nutrient flux to export POC flux in the Eastern Tropical South Pacific, *Mar. Chem.*, *168*, 140–150, doi:10.1016/j.marchem.2014.10.004.
Helber, R. W., R. H. Weisberg, F. Bonjean, E. S. Johnson, and G. S. E. Lagerloef (2007), Satellite-derived surface current divergence in relation to tropical Atlantic SST and wind, *J. Phys. Oceanogr.*, *37*(5), 1357–1375, doi:10.1175/JPO3052.1.
Hendricks, M. B., M. L. Bender, and B. A. Barnett (2004), Net and gross O_2 production in the southern ocean from measurements of biological O_2 saturation and its triple isotope composition, *Deep Sea Res., Part I*, *51*(11), 1541–1561, doi:10.1016/j.dsr.2004.06.006.
Hendricks, M. B., M. L. Bender, B. A. Barnett, P. Strutton, and F. P. Chavez (2005), Triple oxygen isotope composition of dissolved O_2 in the equatorial Pacific: A tracer of mixing, production, and respiration, *J. Geophys. Res.*, *110*, C12021, doi:10.1029/2004JC002735.
Hennon, G. M. M. (2015), Uncovering mechanisms of phytoplankton response to climate change, PhD thesis, School of Oceanography, Univ. of Washington, Seattle, Wash. [Available at http://hdl.handle.net/1773/35281.]
Henson, S. A., R. Sanders, and E. Madsen (2012), Global patterns in efficiency of particulate organic carbon export and transfer to the deep ocean, *Global Biogeochem. Cycles*, *26*, GB1028, doi:10.1029/2011GB004099.
Ho, D. T., R. Wanninkhof, P. Schlosser, D. S. Ullman, D. Hebert, and K. F. Sullivan (2011), Toward a universal relationship between wind speed and gas exchange: Gas transfer velocities measured with ^{3}He/SF_6 during the Southern Ocean gas exchange experiment, *J. Geophys. Res.*, *116*, C00F04, doi:10.1029/2010JC006854.
Howard, E. M. (2017), Ecosystem metabolism in salt marsh tidal creeks and ponds: Applying oxygen isotopes and other gas tracers to novel environments, PhD thesis, Massachusetts Inst. Technol. and Woods Hole Oceanogr. Inst., Cambridge and Woods Hole, Mass. [Available at http://hdl.handle.net/1912/8654.]
Howard, E. M., S. Emerson, S. Bushinsky, and C. Stump (2010), The role of net community production in air-sea carbon fluxes at the North Pacific subarctic-subtropical boundary region, *Limnol. Oceanogr.*, *55*(6), 2585–2596.

Hu, C., E. T. Montgomery, R. W. Schmitt, and F. E. Muller-Karger (2004), The dispersal of the Amazon and Orinoco River water in the tropical Atlantic and Caribbean Sea: Observation from space and S-PALACE floats, *Deep Sea Res., Part II*, *51*(10), 1151–1171, doi:10.1016/j.dsr2.2004.04.001.

Ito, T., C. Deutsch, S. R. Emerson, and R. C. Hamme (2007), Impact of diapycnal mixing on the saturation state of argon in the subtropical North Pacific, *Geophys. Res. Lett.*, *34*, L09602, doi:10.1029/2006GL029209.

Jiao, N., et al. (2010), Microbial production of recalcitrant dissolved organic matter: Long-term carbon storage in the global ocean, *Nature Rev. Microbio.*, *8*, 593–599, doi:10.1038/nrmicro2386.

Johnson, K. S., W. M. Berelson, E. S. Boss, Z. Chase, H. Claustre, S. R. Emerson, N. Gruber, A. Körtzinger, M. J. Perry, and S. C. Riser (2009), Observing biogeochemical cycles at global scales with profiling floats and gliders: Prospects for a global array, *Oceanography*, *22*(3), 216–225, doi:10.5670/oceanog.2009.81.

Juranek, L. W., and P. D. Quay (2013), Using triple isotopes of dissolved oxygen to evaluate global marine productivity, *Annu. Rev. Mar. Sci.*, *5*, 503–524, doi:10.1146/annurev-marine-121211-172430.

Juranek, L. W., R. C. Hamme, J. Kaiser, R. Wanninkhof, and P. D. Quay (2010), Evidence of O_2 consumption in underway seawater lines: Implications for air-sea O_2 and CO_2 fluxes, *Geophys. Res. Lett.*, *37*, L01601, doi:10.1029/2009GL040423.

Juranek, L. W., P. D. Quay, R. A. Feely, D. Lockwood, D. M. Karl, and M. J. Church (2012), Biological production in the NE Pacific and its influence on air-sea CO_2 flux: Evidence from dissolved oxygen isotopes and O_2/Ar, *J. Geophys. Res.*, *117*, C05022, doi:10.1029/2011JC007450.

Kadko, D., and W. Johns (2011), Inferring upwelling rates in the equatorial Atlantic using ^{7}Be measurements in the upper ocean, *Deep Sea Res., Part I*, *58*(6), 647–657, doi:10.1016/j.dsr.2011.03.004.

Kaiser, J. (2011), Technical note: Consistent calculation of aquatic gross production from oxygen triple isotope measurements, *Biogeosciences*, *8*(7), 1793–1811, doi:10.5194/bg-8-1793-2011.

Kaiser, J., and O. Abe (2012), Reply to Nicholson's comment on "Consistent calculation of aquatic gross production from oxygen triple isotope measurements" by Kaiser (2011), *Biogeosciences*, *9*(8), 2921–2933, doi:10.5194/BG-9-2921-2012.

Kaiser, J., M. K. Reuer, B. Barnett, and M. L. Bender (2005), Marine productivity estimates from continuous O_2/Ar ratio measurements by membrane inlet mass spectrometry, *Geophys. Res. Lett.*, *32*, L19605, doi:10.1029/2005GL023459.

Kalnay, E., et al. (1996), The NCEP/NCAR 40-year reanalysis project, *Bull. Am. Meteorol. Soc.*, *77*(3), 437–471, doi:10.1175/1520-0477(1996)077<0437:TNYRP>2.0.CO;2.

Karl, D., R. Bidigare, and R. Letelier (2001), Long-term changes in plankton community structure and productivity in the North Pacific Subtropical Gyre: The domain shift hypothesis, *Deep Sea Res., Part II*, *48*(8), 1449–1470, doi:10.1016/S0967-0645(00)00149-1.

Karl, D. M., M. J. Church, J. E. Dore, R. M. Letelier, and C. Mahaffey (2012), Predictable and efficient carbon sequestration in the North Pacific Ocean supported by symbiotic nitrogen fixation, *Proc. Natl. Acad. Sci.*, *109*(6), 1842–1849, doi:10.1073/pnas.1120312109.

Kavanaugh, M. T., S. R. Emerson, B. Hales, D. M. Lockwood, P. D. Quay, and R. M. Letelier (2014a), Physicochemical and biological controls on primary and net community production across northeast Pacific seascapes, *Limnol. Oceanogr.*, *59*(6), 2013–2027, doi:10.4319/lo.2014.59.6.2013.

Kavanaugh, M. T., B. Hales, M. Saraceno, Y. H. Spitz, A. E. White, and R. M. Letelier (2014b), Hierarchical and dynamic seascapes: A quantitative framework for scaling pelagic biogeochemistry and ecology, *Prog. Oceanogr.*, *120*, 291–304, doi:10.1016/j.pocean.2013.10.013.

Kemp, A. E. S., R. B. Pearce, I. Grigorov, J. Rance, C. B. Lange, P. Quilty, and I. Salter (2006), Production of giant marine diatoms and their export at oceanic frontal zones: Implications for Si and C flux from stratified oceans, *Global Biogeochem. Cycles*, *20*, GB4S04, doi:10.1029/2006GB002698.

Kirk, J. T. O. (1994), *Light and Photosynthesis in Aquatic Ecosystems*, chap. 10, pp. 271–313, Cambridge Univ. Press, Cambridge, U. K.

Klein, P., and G. Lapeyre (2009), The oceanic vertical pump induced by mesoscale and submesoscale turbulence, *Annu. Rev. Mar. Sci.*, *1*(1), 351–375, doi:10.1146/annurev.marine.010908.163704.

Knap, A., A. Michaels, A. Close, H. Ducklow, and A. Dickson (Eds.) (1996), *Protocols for the Joint Global Ocean Flux Study (JGOFS) Core Measurements*, chap. 6, pp. 25–33, Reprint, UNESCO 1994 IOC Manuals and Guides 29, UNESCO, Paris, France.

Knapp, G. P., M. C. Stalcup, and R. J. Stanley (1989), *Dissolved Oxygen Measurements in Sea Water at the Woods Hole Oceanographic Institution*, Full Technical Rep., 14 pp., Woods Hole Oceanographic Institution, Woods Hole, Mass.

Kruskal, W. H., and W. A. Wallis (1952), Use of ranks in one-criterion variance analysis, *J. Am. Stat. Assoc.*, *47*(260), 583, doi:10.2307/2280779.

Kujawinski, E., K. Longnecker (2014), Processed CTD data from all sensors mounted on the rosette from R/V *Knorr* cruise KN210-04 in the western Atlantic Ocean between Uruguay and Barbados in 2013 (Deep Atlantic DOM project), *Biol. Chem. Oceanogr. Data Manag. Off. (BCO-DMO)*. [Available at http://www.bco-dmo.org/project/2204.]

Law, C. S., E. R. Abraham, A. J. Watson, and M. I. Liddicoat (2003), Vertical eddy diffusion and nutrient supply to the surface mixed layer of the Antarctic Circumpolar Current, *J. Geophys. Res.*, *108*(C8), 3272, doi:10.1029/2002JC001604.

Laws, E. A. (1991), Photosynthetic quotients, new production and net community production in the open ocean, *Deep Sea Res., Part A*, *38*(1), 143–167.

Laws, E. A., P. G. Falkowski, W. O. Smith, H. Ducklow, and J. J. McCarthy (2000), Temperature effects on export production in the open ocean, *Global Biogeochem. Cycles*, *14*(4), 1231–1246, doi:10.1029/1999GB001229.

Lê, S., J. Josse, and F. Husson (2008), FactoMineR : An *R* package for multivariate analysis, *J. Stat. Softw.*, *25*(1), doi:10.18637/jss.v025.i01.

Lee, Y. J., et al. (2015), An assessment of phytoplankton primary productivity in the Arctic Ocean from satellite ocean color/in situ chlorophyll-*a* based models, *J. Geophys. Res. Ocean.*, *120*, 6508–6541, doi:10.1002/2015JC011018.

Levitus, S. E. (1982), *Climatological Atlas of the World Ocean*, *NOAA Professional Paper*, vol. 13, U.S. Gov. Print. Off., Washington, D. C.

Lévy, M., R. Ferrari, P. J. S. Franks, A. P. Martin, and P. Rivière (2012), Bringing physics to life at the submesoscale, *Geophys. Res. Lett.*, *39*, L14602, doi:10.1029/2012GL052756.

Lévy, M., O. Jahn, S. Dutkiewicz, and M. J. Follows (2014), Phytoplankton diversity and community structure affected by oceanic dispersal and mesoscale turbulence, *Limnol. Oceanogr. Fluids Environ.*, *4*(1), 67–84, doi:10.1215/21573689-2768549.

Lévy, M., et al. (2015), The dynamical landscape of marine phytoplankton diversity, *J. R. Soc. Interface*, *12*(111), doi:10.1098/rsif.2015.0481.

Lockwood, D., P. D. Quay, M. T. Kavanaugh, L. W. Juranek, and R. A. Feely (2012), High-resolution estimates of net community production and air-sea CO_2 flux in the northeast Pacific, *Global Biogeochem. Cycles*, *26*, GB4010, doi:10.1029/2012GB004380.

Lomas, M. W., and N. R. Bates (2004), Potential controls on interannual partitioning of organic carbon during the winter/spring phytoplankton bloom at the Bermuda Atlantic time-series study (BATS) site, *Deep Sea Res., Part I*, *51*(11), 1619–1636, doi:10.1016/j.dsr.2004.06.007.

Longhurst, A. (1995), Seasonal cycles of pelagic production and consumption, *Prog. Oceanogr.*, *36*(2), 77–167, doi:10.1016/0079-6611(95)00015-1.

Lumpkin, R., and S. L. Garzoli (2005), Near-surface circulation in the tropical Atlantic Ocean, *Deep Sea Res., Part I*, *52*(3), 495–518, doi:10.1016/j.dsr.2004.09.001.

Mahadevan, A. (2016), The impact of submesoscale physics on primary productivity of plankton, *Annu. Rev. Mar. Sci.*, *8*(1), 161–184, doi:10.1146/annurev-marine-010814-015912.
Marañón, E., M. J. Behrenfeld, N. Gonzalez, B. Mourino, and M. V. Zubkov (2003), High variability of primary production in oligotrophic waters of the Atlantic Ocean: Uncoupling from phytoplankton biomass and size structure, *Mar. Ecol. Prog. Ser.*, *257*, 1–11, doi:10.3354/meps257001.
Marra, J. (2002), Approaches to the measurement of plankton production, in *Phytoplankton Productivity*, pp. 78–108, Blackwell Sci., Oxford, U. K.
Marra, J. (2009), Net and gross productivity: Weighing in with ^{14}C, *Aquat. Microb. Ecol.*, *56*(2–3), 123–131, doi:10.3354/ame01306.
Martin, J. H., G. A. Knauer, D. M. Karl, and W. W. Broenkow (1987), VERTEX: Carbon cycling in the northeast Pacific, *Deep Sea Res., Part A*, *34*(2), 267–285, doi:10.1016/0198-0149(87)90086-0.
Martiny, A. C., S. Kathuria, and P. M. Berube (2009), Widespread metabolic potential for nitrite and nitrate assimilation among *Prochlorococcus* ecotypes, *Proc. Natl. Acad. Sci.*, *106*(26), 10,787–10,792, doi:10.1073/pnas.0902532106.
Martz, T. R., K. S. Johnson, and S. C. Riser (2008), Ocean metabolism observed with oxygen sensors on profiling floats in the South Pacific, *Limnol. Oceanogr.*, *53*(5–2), 2094–2111, doi:10.4319/lo.2008.53.5_part_2.2094.
MathWorks (2015), MATLAB and Statistics Toolbox Release 2015b, Software, The MathWorks, Inc., Natick, Mass.
McClain, C. R. (2009), A decade of satellite ocean color observations, *Annu. Rev. Mar. Sci.*, *1*(1), 19–42, doi:10.1146/annurev.marine.010908.163650.
McGillicuddy, D. J. (2016), Mechanisms of physical-biological-biogeochemical interaction at the oceanic mesoscale, *Annu. Rev. Mar. Sci.*, *8*(1), 125–159, doi:10.1146/annurev-marine-010814-015606.
McGillicuddy, D. J., et al. (2007), Eddy/wind interactions stimulate extraordinary mid-ocean plankton blooms, *Science*, *316*(5827), 1021–1026, doi:10.1126/science.1136256.
Mémery, L., M. Arhan, X. Alvarez-Salgado, M.-J. Messias, H. Mercier, C. Castro, and A. Rios (2000), The water masses along the western boundary of the south and equatorial Atlantic, *Prog. Oceanogr.*, *47*(1), 69–98, doi:10.1016/S0079-6611(00)00032-X.
Meyer, J. P., and M. A. Seaman (2013), A comparison of the exact Kruskal-Wallis distribution to asymptotic approximations for all sample sizes up to 105, *J. Exp. Educ.*, *81*(2), 139–156, doi:10.1080/00220973.2012.699904.
Michaels, A. F., and M. W. Silver (1988), Primary production, sinking fluxes and the microbial food web, *Deep Sea Res., Part I*, *35*(4), 473–490, doi:10.1016/0198-0149(88)90126-4.
Mislan, K. A. S., C. A. Stock, J. P. Dunne, and J. L. Sarmiento (2014), Group behavior among model bacteria influences particulate carbon remineralization depths, *J. Mar. Res.*, *72*, 183–218, doi:10.1357/002224014814901985.
Moore, L. R., A. F. Post, G. Rocap, and S. W. Chisholm (2002), Utilization of different nitrogen sources by the marine cyanobacteria *Prochlorococcus* and *Synechococcus*, *Limnol. Oceanogr.*, *47*(4), 989–996, doi:10.4319/lo.2002.47.4.0989.
Moreno-Ostos, E., A. Fernández, M. Huete-Ortega, B. Mouriño-Carballido, A. Calvo-Díaz, X. Anxelu, G. Morán, and E. Marañón (2011), Size-fractionated phytoplankton biomass and production in the tropical Atlantic, *Sci. Mar.*, *75*(752), 379–389, doi:10.3989/scimar.2011.75n2379.
Mouriño-Carballido, B., R. Graña, A. Fernàndez, A. Bode, M. Varela, J. F. Domínguez, J. Escànez, D. de Armas, and E. Marañón (2011), Importance of N_2 fixation vs. nitrate eddy diffusion along a latitudinal transect in the Atlantic Ocean, *Limnol. Oceanogr.*, *56*(3), 999–1007, doi:10.4319/lo.2011.56.3.0999.
Murray, J. W., R. T. Barber, M. R. Roman, M. P. Bacon, and R. A. Feely (1994), Physical and biological controls on carbon cycling in the equatorial pacific, *Science*, *266*(5182), 58–65, doi:10.1126/science.266.5182.58.
Murray, J. W., J. Young, J. Newton, J. Dunne, T. Chapin, B. Paul, and J. J. McCarthy (1996), Export flux of particulate organic carbon from the central equatorial Pacific determined using a combined drifting trap-^{234}Th approach, *Deep Sea Res., Part II*, *43*(4–6), 1095–1132, doi:10.1016/0967-0645(96)00036-7.
Napoléon, C., L. Fiant, V. Raimbault, P. Riou, and P. Claquin (2014), Dynamics of phytoplankton diversity structure and primary productivity in the English Channel, *Mar. Ecol. Prog. Ser.*, *505*, 49–64, doi:10.3354/meps10772.
Nicholson, D., S. Emerson, and C. C. Eriksen (2008), Net community production in the deep euphotic zone of the subtropical North Pacific gyre from glider surveys, *Limnol. Oceanogr.*, *53*(5_part_2), 2226–2236, doi:10.4319/lo.2008.53.5_part_2.2226.
Nicholson, D., R. H. R. Stanley, and S. C. Doney (2014), The triple oxygen isotope tracer of primary productivity in a dynamic ocean model, *Global Biogeochem. Cycles*, *28*, 538–552, doi:10.1002/2013GB004704.
Nicholson, D. P. (2011), Comment on: "Technical note: Consistent calculation of aquatic gross production from oxygen triple isotope measurements" by Kaiser (2011), *Biogeosciences*, *8*, 2993–2997, doi:10.5194/bg-8-2993-2011.
Nicholson, D. P., S. R. Emerson, S. Khatiwala, and R. Hamme (2011), An inverse approach to estimate bubble-mediated air-sea gas flux from inert gas measurements, in *Proceedings on the 6th International Symposium on Gas Transfer at Water Surfaces*, pp. 223–237, Kyoto Univ. Press, Kyoto, Japan.
Nicholson, D. P., R. H. R. Stanley, E. Barkan, D. M. Karl, B. Luz, P. D. Quay, and S. C. Doney (2012), Evaluating triple oxygen isotope estimates of gross primary production at the Hawaii Ocean time-series and Bermuda Atlantic time-series study sites, *J. Geophys. Res.*, *117*, C05012, doi:10.1029/2010JC006856.
Nicholson, D. P., S. T. Wilson, S. C. Doney, and D. M. Karl (2015), Quantifying subtropical North Pacific gyre mixed layer primary productivity from Seaglider observations of diel oxygen cycles, *Geophys. Res. Lett.*, *42*, 4032–4039, doi:10.1002/2015GL063065.
Oksanen, J., et al. (2016), Vegan: Community ecology package, software. [Available at https://cran.r-project.org/web/packages/vegan/index.html.]
Ostle, C., M. Johnson, P. Landschützer, U. Schuster, S. Hartman, T. Hull, and C. Robinson (2015), Net community production in the North Atlantic Ocean derived from volunteer observing ship data, *Global Biogeochem. Cycles*, *29*, 80–95, doi:10.1002/2014GB004868.
Owens, S. A., S. Pike, and K. O. Buesseler (2015), Thorium-234 as a tracer of particle dynamics and upper ocean export in the Atlantic Ocean, *Deep Sea Res., Part II*, *116*, 42–59, doi:10.1016/j.dsr2.2014.11.010.
Palevsky, H. I., P. D. Quay, and D. P. Nicholson (2016), Discrepant estimates of primary and export production from satellite algorithms, a biogeochemical model, and geochemical tracer measurements in the North Pacific Ocean, *Geophys. Res. Lett.*, *43*, 8645–8653, doi:10.1002/2016GL070226.
Palevsky, H. I., F. Ribalet, J. E. Swalwell, C. E. Cosca, E. D. Cokelet, R. A. Feely, E. V. Armbrust, and P. D. Quay (2013), The influence of net community production and phytoplankton community structure on CO_2 uptake in the Gulf of Alaska, *Global Biogeochem. Cycles*, *27*, 664–676, doi:10.1002/gbc.20058.
Palter, J. B., I. Marinov, J. L. Sarmiento, and N. Gruber (2013), Large-scale, persistent nutrient fronts of the World Ocean: Impacts on biogeochemistry, in *Chemical Oceanography of Frontal Zones*, edited by I. Belkin, 38 pp., pp. 1–38, Springer, Berlin.

Peterson, R. G., and L. Stramma (1991), Upper-level circulation in the South Atlantic Ocean, *Prog. Oceanogr.*, *26*(1), 1–73, doi:10.1016/0079-6611(91)90006-8.

Plattner, G.-K., N. Gruber, H. Frenzel, and J. C. McWilliams (2005), Decoupling marine export production from new production, *Geophys. Res. Lett.*, *32*, L11612, doi:10.1029/2005GL022660.

Pollard, R. T., et al. (2009), Southern Ocean deep-water carbon export enhanced by natural iron fertilization, *Nature*, *457*(7229), 577–580, doi:10.1038/nature07716.

Poulton, A. J., P. M. Holligan, A. Hickman, Y.-N. Kim, T. R. Adey, M. C. Stinchcombe, C. Holeton, S. Root, and E. M. S. Woodward (2006), Phytoplankton carbon fixation, chlorophyll-biomass and diagnostic pigments in the Atlantic Ocean, *Deep Sea Res., Part II*, *53*(14–16), 1593–1610, doi:10.1016/j.dsr2.2006.05.007.

Prokopenko, M. G., O. M. Pauluis, J. Granger, and L. Y. Yeung (2011), Exact evaluation of gross photosynthetic production from the oxygen triple-isotope composition of O_2: Implications for the net-to-gross primary production ratios, *Geophys. Res. Lett.*, *38*, L14603, doi:10.1029/2011GL047652.

Quay, P., J. Stutsman, and T. Steinhoff (2012), Primary production and carbon export rates across the subpolar N. Atlantic Ocean basin based on triple oxygen isotope and dissolved O_2 and Ar gas measurements, *Global Biogeochem. Cycles*, *26*, GB2003, doi:10.1029/2010GB004003.

Reuer, M. K., B. A. Barnett, M. L. Bender, P. G. Falkowski, and M. B. Hendricks (2007), New estimates of Southern Ocean biological production rates from O_2/Ar ratios and the triple isotope composition of O_2, *Deep Sea Res., Part I*, *54*(6), 951–974, doi:10.1016/j.dsr.2007.02.007.

Reygondeau, G., A. Longhurst, E. Martinez, G. Beaugrand, D. Antoine, and O. Maury (2013), Dynamic biogeochemical provinces in the global ocean, *Global Biogeochem. Cycles*, *27*, 1046–1058, doi:10.1002/gbc.20089.

Rhein, M., M. Dengler, J. Sültenfuß, R. Hummels, S. Hüttl-Kabus, and B. Bourles (2010), Upwelling and associated heat flux in the equatorial Atlantic inferred from helium isotope disequilibrium, *J. Geophys. Res.*, *115*, C08021, doi:10.1029/2009JC005772.

Ribalet, F., A. Marchetti, K. A. Hubbard, K. Brown, C. A. Durkin, R. Morales, M. Robert, J. E. Swalwell, P. D. Tortell, and E. V. Armbrust (2010), Unveiling a phytoplankton hotspot at a narrow boundary between coastal and offshore waters, *Proc. Natl. Acad. Sci.*, *107*(38), 16,571–16,576, doi:10.1073/pnas.1005638107.

Richardson, T. L., and G. A. Jackson (2007), Small phytoplankton and carbon export from the surface ocean, *Science*, *315*(5813), 838–840, doi:10.1126/science.1133471.

Robinson, C., et al. (2006), The Atlantic Meridional Transect (AMT) programme: A contextual view 1995–2005, *Deep Sea Res., Part II*, *53*(14–16), 1485–1515, doi:10.1016/j.dsr2.2006.05.015.

Robinson, C., P. Holligan, T. Jickells, and S. Lavender (2009), The Atlantic Meridional Transect programme (1995–2012), *Deep Sea Res., Part II*, *56*(15), 895–898, doi:10.1016/j.dsr2.2008.10.005.

Romera-Castillo, C., R. T. Letscher, and D. A. Hansell (2016), New nutrients exert fundamental control on DOC accumulation in the surface Atlantic Ocean, *Proc. Natl. Acad. Sci.*, *113*(38), doi:10.1073/pnas.1605344113.

Sarma, V. V. S. S., O. Abe, A. Hinuma, and T. Saino (2006), Short-term variation of triple oxygen isotopes and gross oxygen production in the Sagami Bay, central Japan, *Limnol. Oceanogr.*, *51*(3), 1432–1442, doi:10.4319/lo.2006.51.3.1432.

Schlitzer, R. (2015), Ocean data view. [Available at http://odv.awi.de.]

Schmidtko, S., G. C. Johnson, and J. M. Lyman (2013), MIMOC: A global monthly isopycnal upper-ocean climatology with mixed layers, *J. Geophys. Res. Ocean.*, *118*, 1658–1672, doi:10.1002/jgrc.20122.

Scholz, F. W., and M. A. Stephens (1987), K-sample Anderson-Darling tests, *J. American Stats. Assoc.*, *399*, 918–924, doi:10.1080/01621459.1987.10478517.

Serret, P., C. Robinson, M. Aranguren-Gassis, E. E. García-Martín, N. Gist, V. Kitidis, J. Lozano, J. Stephens, C. Harris, and R. Thomas (2015), Both respiration and photosynthesis determine the scaling of plankton metabolism in the oligotrophic ocean, *Nat. Commun.*, *6*, doi:10.1038/ncomms7961.

Šidák, Z. (1967), Rectangular confidence regions for the means of multivariate normal distributions, *J. Am. Stat. Assoc.*, *62*(318), 626–633, doi:10.1080/01621459.1967.10482935.

Siegel, D. A., K. O. Buesseler, S. C. Doney, S. F. Sailley, M. J. Behrenfeld, and P. W. Boyd (2014), Global assessment of ocean carbon export by combining satellite observations and food-web models, *Global Biogeochem. Cycles*, *28*, 181–196, doi:10.1002/2013GB004743.

Siegel, D. A., E. Fields, and K. O. Buesseler (2008), A bottom-up view of the biological pump: Modeling source funnels above ocean sediment traps, *Deep Sea Res., Part II*, *55*(1), 108–127, doi:10.1016/j.dsr.2007.10.006.

Spitzer, W. S., and W. J. Jenkins (1989), Rates of vertical mixing, gas exchange and new production: Estimates from seasonal gas cycles in the upper ocean near Bermuda, *J. Mar. Res.*, *47*(1), 169–196, doi:10.1357/002224089785076370.

Stanley, R. H. R., and E. M. Howard (2013), Quantifying photosynthetic rates of microphytobenthos using the triple isotope composition of dissolved oxygen, *Limnol. Oceanogr. Methods*, *11*, 360–373.

Stanley, R. H. R., W. J. Jenkins, D. E. Lott, and S. C. Doney (2009), Noble gas constraints on air-sea gas exchange and bubble fluxes, *J. Geophys. Res.*, *114*, C11020, doi:10.1029/2009JC005396.

Stanley, R. H. R., J. B. Kirkpatrick, N. Cassar, B. A. Barnett, and M. L. Bender (2010), Net community production and gross primary production rates in the western equatorial Pacific, *Global Biogeochem. Cycles*, *24*, GB4001, doi:10.1029/2009GB003651.

Steinberg, D. K., C. A. Carlson, N. R. Bates, S. A. Goldthwait, L. P. Madin, and A. F. Michaels (2000), Zooplankton vertical migration and the active transport of dissolved organic and inorganic carbon in the Sargasso Sea, *Deep Sea Res., Part I*, *47*(1), 137–158, doi:10.1016/S0967-0637(99)00052-7.

Steinberg, D. K., C. A. Carlson, N. R. Bates, R. J. Johnson, A. F. Michaels, and A. H. Knap (2001), Overview of the US JGOFS Bermuda Atlantic Time-series Study (BATS): A decade-scale look at ocean biology and biogeochemistry, *Deep Sea Res., Part II*, *48*(8), 1405–1447, doi:10.1016/S0967-0645(00)00148-X.

Stramma, L., and F. Schott (1999), The mean flow field of the tropical Atlantic Ocean, *Deep Sea Res., Part II*, *46*(1–2), 279–303, doi:10.1016/S0967-0645(98)00109-X.

Stukel, M. R., M. Kahru, C. R. Benitez-Nelson, M. Décima, R. Goericke, M. R. Landry, and M. D. Ohman (2015), Using Lagrangian-based process studies to test satellite algorithms of vertical carbon flux in the eastern North Pacific Ocean, *J. Geophys. Res. Ocean.*, *120*, 7208–7222, doi:10.1002/2015JC011264.

Stukel, M. R., and M. R. Landry (2010), Contribution of picophytoplankton to carbon export in the equatorial Pacific: A reassessment of food web flux inferences from inverse models, *Limnol. Oceanogr.*, *55*(6), 2669–2685, doi:10.4319/LO.2010.55.6.2669.

Swalwell, J. E., F. Ribalet, and E. V. Armbrust (2011), SeaFlow: A novel underway flow-cytometer for continuous observations of phytoplankton in the ocean, *Limnol. Oceanogr. Methods*, *9*(10), 466–477, doi:10.4319/lom.2011.9.466.

Sweeney, E. N., D. J. McGillicuddy, and K. O. Buesseler (2003), Biogeochemical impacts due to mesoscale eddy activity in the Sargasso Sea as measured at the Bermuda Atlantic Time-series Study (BATS), *Deep Sea Res., Part II*, *50*(22), 3017–3039, doi:10.1016/j.dsr2.2003.07.008.

Świrgoń, M., and M. Stramska (2015), Comparison of in situ and satellite ocean color determinations of particulate organic carbon concentration in the global ocean, *Oceanologia*, *57*(1), 25–31, doi:10.1016/j.oceano.2014.09.002.

Takahashi, T., et al. (2009), Climatological mean and decadal change in surface ocean pCO_2, and net sea–air CO_2 flux over the global oceans, *Deep Sea Res., Part II*, *56*(8), 554–577, doi:10.1016/j.dsr2.2008.12.009.

Thomalla, S., R. Turnewitsch, M. Lucas, and A. Poulton (2006), Particulate organic carbon export from the North and South Atlantic gyres: The $^{234}Th/^{238}U$ disequilibrium approach, *Deep Sea Res., Part II*, *53*(14), 1629–1648, doi:10.1016/j.dsr2.2006.05.018.

Tilstone, G., T. Smyth, A. Poulton, and R. Hutson (2009), Measured and remotely sensed estimates of primary production in the Atlantic Ocean from 1998 to 2005, *Deep Sea Res., Part II*, *56*(15), 918–930, doi:10.1016/j.dsr2.2008.10.034.

Tilstone, G.H., Y.-y. Xie, C. Robinson, P. Serret, D.E. Raitsos, T. Powell, M. Aranguren-Gassis, E.E. Garcia-Martin, and V. Kitidis (2015), Satellite estimates of net community production indicate predominance of net autotrophy in the Atlantic Ocean, *Remote Sens. Envir.*, *164*, 254–269, doi:10.1016/j.rse.2015.03.017.

Trujillo-Ortiz, A., R. Hernandez-Walls, K. Barba-Rojo, and A. Castro-Perez (2007), ANDARTEST Anderson-Darling test for assessing normality of a sample data, software. [Available at http://www.mathworks.com/matlabcentral/.]

Tsuchiya, M., L. D. Talley, and M. S. McCartney (1994), Water-mass distributions in the western South Atlantic; a section from South Georgia Island (54S) northward across the equator, *J. Mar. Res.*, *52*(1), 55–81, doi:10.1357/0022240943076759.

Uitz, J., H. Claustre, B. Gentili, and D. Stramski (2010), Phytoplankton class-specific primary production in the world's oceans: Seasonal and interannual variability from satellite observations, *Global Biogeochem. Cycles*, *24*, GB3016, doi:10.1029/2009GB003680.

Vaillancourt, R. D., J. Marra, M. P. Seki, M. L. Parsons, and R. R. Bidigare (2003), Impact of a cyclonic eddy on phytoplankton community structure and photosynthetic competency in the subtropical North Pacific Ocean, *Deep Sea Res., Part I*, *50*(7), 829–847, doi:10.1016/S0967-0637(03)00059-1.

Volk, T., and M. I. Hoffert (1985), Ocean carbon pumps: Analysis of relative strengths and efficiencies in ocean-driven atmospheric CO2 changes, in *The Carbon Cycle and Atmospheric CO_2: Natural Variations Archean to Present*, *Geophys. Monogr. Ser.*, edited by E. T. Sundquist and W. S. Broecker, AGU, Washington, D. C., doi:10.1029/GM032p0099.

Wanninkhof, R. (2014), Relationship between wind speed and gas exchange over the ocean revisited, *Limnol. Oceanogr. Methods*, *12*(6), 351–362, doi:10.4319/lom.2014.12.351.

Westberry, T., M. J. Behrenfeld, D. A. Siegel, and E. Boss (2008), Carbon-based primary productivity modeling with vertically resolved photoacclimation, *Global Biogeochem. Cycles*, *22*, GB2024, doi:10.1029/2007GB003078.

Williams, P. J. L. (1993), On the definition of plankton production terms, *ICES Mar. Sci. Symp.*, *197*, 9–19.

Williams, P. J. l. B., and D. Lefèvre (1996), Algal ^{14} C and total carbon metabolisms. 1. Models to account for the physiological processes of respiration and recycling, *J. Plankton Res.*, *18*(10), 1941–1959, doi:10.1093/plankt/18.10.1941.

Wilson, C., T. A. Villareal, N. Maximenko, S. J. Bograd, J. P. Montoya, and C. A. Schoenbaechler (2008), Biological and physical forcings of late summer chlorophyll blooms at 30°N in the oligotrophic Pacific, *J. Mar. Syst.*, *69*(3), 164–176, doi:10.1016/j.jmarsys.2005.09.018.

Wunsch, C., and R. Ferrari (2004), Vertical mixing, energy, and the general circulation of the oceans, *Annu. Rev. Fluid Mech.*, *36*(1), 281–314, doi:10.1146/annurev.fluid.36.050802.122121.

Xing, X., A. Morel, H. Claustre, D. Antoine, F. D'Ortenzio, A. Poteau, and A. Mignot (2011), Combined processing and mutual interpretation of radiometry and fluorimetry from autonomous profiling Bio-Argo floats: Chlorophyll *a* retrieval, *J. Geophys. Res.*, *116*, C06020, doi:10.1029/2010JC006899.

Yeung, L. Y., et al. (2012), Impact of diatom-diazotroph associations on carbon export in the Amazon River plume, *Geophys. Res. Lett.*, *39*, L18609, doi:10.1029/2012GL053356.

Yoder, J. A., S. G. Ackleson, R. T. Barber, P. Flament, and W. M. Balch (1994), A line in the sea, *Nature*, *371*(6499), 689–692, doi:10.1038/371689a0.

Zehr, J. P., E. J. Carpenter, and T. A. Villareal (2000), New perspectives on nitrogen-fixing microorganisms in tropical and subtropical oceans, *Trends Microbiol.*, *8*(2), 68–73, doi:10.1016/S0966-842X(99)01670-4.

Zhang, X., and H. G. Dam (1997), Downward export of carbon by diel migrant mesozooplankton in the central equatorial Pacific, *Deep Sea Res., Part II*, *44*(9–10), 2191–2202, doi:10.1016/S0967-0645(97)00060-X.